Chapter 3
One-Dimensional Model of Water Quality and Aquatic Ecosystem/Ecotoxicology in River Systems

Podjanee Inthasaro and Weiming Wu

Contents

Abstract A one-dimensional water quality and aquatic ecology/ecotoxicology model has been incorporated into a package for the modeling of hydrodynamic, sediment transport, contaminant transport, water quality, aquatic ecosystem, and ecotoxicology in river systems. The water quality model alone can be used to determine water temperature, dissolved oxygen, biological oxygen demand, nitrogen, phosphorus, and conservative chemical such as chloride. The aquatic ecosystem model considers a basic food web structure consisting of four trophic

P. Inthasaro, Ph.D.
Previously at, 1157 Crane Crest Way, Orlando, FL 32825, USA
e-mail: pinthasaro@gmail.com

W. Wu, Ph.D. (✉)
Department of Civil and Environmental Engineering,
Wallance H. Coulter School of Engineering, Clarkson University, Box 5710,
8 Clarkson Avenue, Potsdam, NY 13699, USA
e-mail: wwu@clarkson.edu

L.K. Wang, C.T. Yang, and M.-H.S. Wang (eds.), *Advances in Water Resources Management*, Handbook of Environmental Engineering, Volume 16,
DOI 10.1007/978-3-319-22924-9_3

levels: phytoplankton, zooplankton, forage fish, and predatory fish, undergoing various biological processes such as photosynthesis, grazing, respiration, excretion, defecation, mortality, gamete, and reproduction. The model simulates the bioaccumulation of toxic chemicals in organisms by uptake, depuration and dietary, and takes into account the effects of toxicity on organisms through modification factors of photosynthesis, grazing, and gamete mortality. The modeling package has been tested by simulating the water quality parameters in the Tualatin River, Oregon and the water quality, aquatic ecosystem, polychlorinated biphenyl (PCB) transport and bioaccumulation in the Upper Hudson River, New York. The simulated water quality parameters, phytoplankton and zooplankton biomass, fish populations, and PCB concentrations in fish are in generally good agreement with the measurement data.

Keywords Water quality model • Aquatic ecosystem model • Ecotoxicology model • Freshwater riverine system • Contaminant transport • Food web

Nomenclature

$[H]^+$	Molar concentration of hydrogen ion, mol/m^3
$[OH]^-$	Molar concentration of hydroxide ion, mol/m^3
A	Cross-sectional flow area, m^2
C_a	Biomass concentration of phytoplankton, g/m^3, or μg/L
c_b	Bowen coefficient
C_{CBOD}	Concentration of carbonaceous biological oxygen demand (CBOD), g/m^3
C_{DO}	Dissolved oxygen (DO) concentration, g/m^3
C'_{DO}	Saturation DO concentration, g/m^3
C_g	Gas-phase concentration of the contaminant, g/m^3
C_L	Fraction of cloud cover
C_m	Concentration of suspended solid, g/m^3
C_{NH3}	Concentration of ammonia nitrogen, g/m^3
C_{NO3}	Concentration of nitrate nitrogen, g/m^3
C_{ON}	Concentration of organic nitrogen, g/m^3
C_{OP}	Concentration of organic phosphorus, g/m^3
c_p	Specific heat capacity
C_{PO4}	Concentration of orthophosphate, g/m^3
$C_{tb,i}$	Total concentration of contaminant in bed layer i
C_{ti}	Contaminant concentration associated with organism i in unit volume of water column, g/m^3
C_{tw}	Total concentration of contaminant in the water column, g/m^3
D_b	Sediment deposition rate, m/d
D_x	Longitudinal dispersion coefficient, m^2/s
e_{air}	Air vapor pressure, mb

ε_{air} Emissivity value of air
E_b Sediment erosion rate, m/d
e_s Saturation vapor pressure, mb
ε_{water} Emissivity value of water
f_{act} Factor for respiratory rate associated with swimming or active respiratory fraction
$f_{db,1}$ Fraction of dissolved contaminant in bed surface layer
f_{den} Density-dependent respiration factor
f_{dw} Fraction of dissolved concentration to the total concentration of contaminant in water column
f_{dyn} Proportion of assimilated energy lost to specific dynamic action
f'_{ib} Increase factor in the gamete due to toxic chemicals
f'_{ig} Reduction factor in animal growth due to toxic chemicals
f_{ij} Relative preference factor of predator j feeding on organism i as food
f_L Light limitation factor
f_N Nutrient limitation factor
f_{NH3} Fraction of ammonia in dead organic material
f_{pb} Fraction of particulate contaminant in the bed sediment
f_{PBOD} Fraction of particulate CBOD in total CBOD
f_{PO4} Fraction of phosphate in dead organic material
f_{PON} Fraction of particulate organic nitrogen to organic nitrogen
f_{POP} Fraction of particulate organic phosphorus to organic phosphorus
f_{pw} Fraction of particulate contaminant in the water column
f_{shade} Shading factor defined as the fraction of potential solar radiation that is blocked due to riparian vegetation and landscape
f_T Temperature limitation factor
f_{TOX} Reduction factor due to toxic chemicals
H Henry's law constant, atm m^3/mol
h_{CBOD} Half-saturation DO concentration for CBOD decay, g/m^3
h_L Half-saturation light intensity for phytoplankton growth
h_N Half-saturation concentration for nitrogen, g/m^3
h_N Michaelis–Menten constant for nitrogen uptake, mgN/L
h_{NH3} Half-saturation DO concentration for nitrification, g/m^3
h_{NO3} Half-saturation DO concentration for denitrification, g/m^3
h_{OP} Half-saturation phytoplankton conc. for mineralization of phosphorus, g/m^3
h_P Half-saturation concentration for phosphorus, g/m^3
I_0 Light intensity at the water surface
IC_{i50} Internal concentration of the contaminant in the biotic organism
J_{dbw} Vertical diffusion fluxes between water column and bed surface layer, g/m^2d
K_b Biodegradation rate, 1/d
K_{CBOD} CBOD decay rate, 1/d
K_d Sorption–desorption coefficient, m^3/g

$k_{dbi,i+1}$ Diffusional transfer coefficient of dissolved contaminant between layers i and i + 1
k_{dbw} Diffusional transfer coefficient of dissolved contaminant across the bed surface
K_H Acid-catalyzed hydrolysis rate, m^3/mold
K_i Carrying capacity of fish i, g/m^3
K_{i1} Uptake rate of contaminant of organism i, 1/d
K_{i2} Depuration rate of contaminant of organism i, 1/d
K_{ib} Gamete loss rate of organism i, 1/d
K_{ib0} Intrinsic gamete mortality rate, 1/d
K_{id} Defecation rate of biotic organism i, 1/d
K_{ie} Excretion rate of biotic organism i, 1/d
$K_{ie,max}$ Maximum rate of excretion of organism i, 1/d
K_{ig} Grazing rate of organism i, 1/d
$K_{ig,max}$ Maximum grazing rate of organism i, 1/d
K_{im} Nonpredatory mortality rate of organism i, 1/d
$K_{im,max}$ Maximum rate of nonpredatory mortality of organism i, 1/d
K_{ir} Respiration rate of biotic organism i, 1/d
$K_{ir,max}$ Maximum respiration rate of organism i, 1/d
K_{ir0} Basal or standard respiratory rate, 1/d
K_{ire} Reproduction rate of organism i, 1/d
K_N Neutral hydrolysis rate, 1/d
K_{NH3} Nitrification rate, 1/d
K_{NO3} Denitrification rate, 1/d
K_{OH} Base-catalyzed hydrolysis rate, m^3/mol d
K_{ON} Mineralization rate of organic nitrogen, 1/d
K_{OP} Mineralization rate of organic phosphorus, 1/d
K_p Photolysis rate, 1/d
K_{RE} Depth-averaged reaeration rate, 1/d
$k_{tb,i}$ Decay coefficient of contaminant at layer i
KT_{g1} Coefficient representing the relationships of growth on temperature below the optimal temperature
KT_{g2} Coefficient representing the relationships of growth on temperature above the optimal temperature
K_v Volatilization rate, m/d
LC_{i50} Internal concentration (the concentration of contaminant in water that causes 50 % mortality for a given period of exposure)
m Suspended sediment concentration by volume
p_{ji} Preference of predator i feeding on organism j as food
p_{NH3} Ammonia preference factor
Q Flow discharge, m^3/s
q_l Latent heat flux
q_{lw} Long-wave atmospheric radiation
q_s Convective heat flux
q_{sw} Solar radiation

$q_{sw,clear}$	Short-wave radiation reaching the water surface on a clear day after atmospheric attenuation
$q_{t,ex}$	Total exchange rate of contaminant due to sediment erosion and deposition, g/m^{2}d
$q_{tbi,i+1}$	Total exchange rate of contaminant between layers i and i + 1 due to lowering and rising of the interface
q_{tw}	Total loading rate of contaminant per unit volume, g/m^{3}d
R	Universal gas constant, atm m^3/mol °K
R_{lw}	Reflectivity of water surface for long-wave radiation
R_{sw}	Albedo or reflection coefficient
S_{SOD}	Sediment oxygen demand flux, g/m^{2}s
t	Time, s
T	Water temperature, °C
t_1	Exposure time in toxicity test
t_2	Period of exposure
T_{air}	Air temperature, °K
T_K	Water temperature in °K
T_{opt}	Optimal temperature for biological growth
T_{water}	Water temperature, °K or °C
U	Flow velocity, m/s
α	Velocity correction coefficient
α_{NC}	Stoichiometric ratio of nitrogen to carbon, gN/gC
α_{PC}	Stoichiometric ratio of phosphorus to carbon, gP/gC
γ	Light extinction, 1/m
γ_0	Background light extinction, 1/m
δ_i	Thickness of layer i
θ	Temperature coefficient
λ_i	Grazing limitation factor
ν_i	Concentration of contaminant in biotic organism i, g/g
ρ	Water density, kg/m^3
ρ_d	Dry density of the bed sediment, g/m^3
σ	Stefan–Boltzmann constant, W/m^2 °K^4
ϕ	Porosity
ω_a	Settling velocity of phytoplankton, m/d
ω_{CBOD}	Settling velocity of CBOD, m/s
ω_{ON}	Settling velocity of organic nitrogen, m/s
ω_{OP}	Settling velocity of organic phosphorus, m/s

1 Introduction

During the past decades, many streams and rivers all over the world have been impacted by point and nonpoint source pollutants from residential area, industry, agriculture and so on. Human or animals can be exposed to the toxic pollutants

through food chains in the ecosystems and experience health problems. Because ecosystems are highly dependent on the hydrodynamic, morphodynamic and water quality factors and a large number of physical, chemical, biological, and ecological processes are involved, it is desired to study the integrated dynamics of flow, sediment transport, water quality, aquatic ecosystem, and ecotoxicology in river systems. Simulation of them is quite challenging but important.

Most of the early water quality models focused on dissolved oxygen (DO) and biological oxygen demand (BOD) and launched with the Streeter–Phelps simple BOD–DO model [1]. Then, the models evolved to investigate eutrophication for environmental management by incorporating more processes and components that influence water quality and cope with complex hydrodynamics. In recent years, because of advanced computer technology and increased public health and environmental awareness, several well-established water quality models have become available, such as the Water Quality Analysis Simulation Program (WASP) [2, 3], the river and stream water quality model QUAL2K [4], the multi-dimensional water quality model CE-QUAL-ICM [5], and CCHE_WQ [6]. Further developments have led to a number of aquatic ecological models which represent biotic and abiotic structures in combination with physical, chemical, biological, and ecological processes. Examples of well-established aquatic ecosystem models are Ecopath with Ecosim (EwE) [7], the Computational Aquatic Ecosystem Dynamics Model (CAEDYM) [8], EcoNetwrk [9], and AQUATOX [10, 11]. A recent review of the state of the art for water quality modeling can be found at [12, 13].

Among the above-mentioned water quality and ecosystem models, WASP and AQUATOX are two versatile programs and have been applied widely. Recent studies for model applications include [14–19]. WASP can simulate both phytoplankton and benthic algae in an eutrophication system, but it does not include higher trophic compartments such as zooplankton and fish. In contrast, AQUATOX has a robust aquatic ecosystem model that can simulate a complex aquatic food web with age-structure and trophic interactions. WASP can perform channel flow calculations itself or be linked to external hydrodynamic models such as the Environmental Fluid Dynamics Code (EFDC), the hydrodynamic program DYNHYD, RIVMOD, and the one-dimensional dynamic flow and water quality model CE-QUAL-RIV1 [20]. Similar to WASP, AQUATOX is linked to the Hydrological Simulation Program—Fortran (HSPF) for external hydrodynamic computation. Recently, AQUATOX introduced the multi-segment version which includes linkage of individual AQUATOX segments into a single simulation [11]. However, both models do not have robust sediment transport models. Although AQUATOX is a powerful tool for the simulation of aquatic ecosystems, it involves a large number of variables and parameters that can possibly be used only by experienced users [21]. To reduce the complexity of AQUATOX and incorporate water quality computations from WASP, a new water quality and aquatic ecosystem/ecotoxicology model has been developed in this study.

The present water quality and ecological model is intended for prediction of riverine ecosystems with the effects of toxic chemicals. The model schemes are developed by adopting the merits of the water quality model WASP and the aquatic

ecosystem model AQUATOX. The developed water quality model simulates the temporal and spatial variations of water temperature, conservative substances such as chloride, and non-conservative substances such as dissolved oxygen, biological oxygen demand, nitrogen, and phosphorus. The aquatic food web model simulates dynamic interactions of phytoplankton, zooplankton, forage fish, and predatory fish. The model can compute the fate and transport of a contaminant in water column and sediment bed. The bioaccumulation model involves the direct transfer of the contaminant from water through surface sorption or gill uptake and the accumulation throughout the trophic levels of the food web. The governing equations, kinetic relations, numerical solution algorithms and tests of the developed model are presented in the following sections.

2 Governing Equations

The model simulates the fate and transport of constituents carried by water and/or sediment in channel networks. The present model is developed as an add-on to the existing 1-D flow and sediment transport model, CCHE1D [22]. CCHE1D is a one-dimensional channel-network hydrodynamic and sediment transport model, which was developed and maintained by the National Center for Computational Hydroscience and Engineering (NCCHE) of the University of Mississippi. The CCHE1D flow model simulates unsteady flow in channels of compound cross-sections, accounting for in-stream hydraulic structures. The sediment transport model computes the non-equilibrium transport of non-uniform sediment mixtures. The flow is governed by the 1-D St. Venant equations and the multiple-sized sediment transport is described by a non-equilibrium total-load transport equation. The flow and sediment transport equations and the corresponding numerical solution procedures refer to [22]. The transport of a constituent in the water quality and ecosystem is described by the following advection–dispersion equation:

$$A\frac{DC}{Dt} = \frac{\partial(AC)}{\partial t} + \frac{\partial(\alpha QC)}{\partial x} - \frac{\partial}{\partial x}\left(D_x A \frac{\partial C}{\partial x}\right) = AS \tag{3.1}$$

where

t = time, s
x = coordinate along the channel, m
A = cross-sectional flow area, m^2
Q = flow discharge, m^3/s
C = concentration of the constituent in water column, g/m^3
D_x = longitudinal dispersion coefficient, m^2/s
S = net source/sink term due to biochemical and physical processes and/or due to lateral input to the channel by runoff, g/m^3s
α = velocity correction coefficient.

Equation (3.1) is a general transport equation. The constituent can be any substance transporting in the water column, including sediment, heat (water temperature), pollutants, dissolved oxygen, nitrogen, phosphorus, phytoplankton, zooplankton, and fish. The coefficient α is given a value of 1 for the water quality constituents, phytoplankton, zooplankton and small fish which are assumed to move with the flow, whereas α is set as 0 for large fish which is assumed to move randomly in the domain in the present study. The value of α for migration fish needs to be investigated further. In addition, large fish does not experience the turbulent diffusion or mechanical dispersion as the water quality constituents do, but this difference is ignored for simplicity because the dispersion term is usually much smaller than the advection term in 1-D river systems.

Note that Eq. (3.1) also defines the operator (DC/Dt), which represents the storage, convection and dispersion terms divided by A.

3 Numerical Procedures

Equation (3.1) is discretized using a finite-volume scheme. The control volume for point i is embraced by faces i − 1/2 and i + 1/2 as shown in Fig. 3.1. For α = 1.0, Eq. (3.1) is integrated over the control volume as [23]

$$\frac{(A_iC_i)^{n+1} - (A_iC_i)^n}{\Delta t}\Delta x + \left(QC - AD_x\frac{\partial C}{\partial x}\right)_{i+1/2}^{n+1} - \left(QC - AD_x\frac{\partial C}{\partial x}\right)_{i-1/2}^{n+1} = A_i^{n+1}S_i^{n+1}\Delta x \tag{3.2}$$

where

Δx = length of the control volume
Δt = computational time step
n = superscript which denotes time level
i = subscript which denotes grid point.

Using the analytical solution expressions of the steady, homogeneous, linearized form of Eq. (3.1) in the control volume, Eq. (3.2) is reformulated as

$$a_iC_i = a_{i+1}C_{i+1} + a_{i-1}C_{i-1} + b \tag{3.3}$$

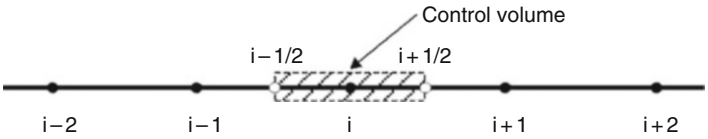

Fig. 3.1 1-D finite volume mesh

$$a_{i+1} = \left(\frac{Q_{i+1/2}}{\exp\left[(U/D_x)_{i+1/2} (x_{i+1} - x_i) \right] - 1} \right)^{n+1} \tag{3.4}$$

$$a_{i-1} = \left(\frac{Q_{i-1/2}}{\exp\left[(U/D_x)_{i-1/2} (x_i - x_{i-1}) \right] - 1} + Q_{i-1/2} \right)^{n+1} \tag{3.5}$$

$$a_i = a_{i+1} + a_{i-1} + Q_{i+1/2}^{n+1} - Q_{i-1/2}^{n+1} + A_i^{n+1} \frac{\Delta x}{\Delta t} \tag{3.6}$$

$$b = S_i^{n+1} A_i^{n+1} \Delta x + A_i^n \frac{\Delta x}{\Delta t} C_i^n \tag{3.7}$$

where

U = flow velocity.

When $\alpha = 0$, Eq. (3.1) becomes a diffusion-type equation. The dispersion term can be discretized using the central difference scheme. The final discretized equation can be written as Eq. (3.3) with different coefficients.

The discretized equations at the internal control volumes and boundary conditions at the inlet and outlet form a system of algebraic equations with a tridiagonal coefficient matrix, which can be solved using the Thomas algorithm, also called TDMA (TriDiagonal Matrix Algorithm). The details can be found in many text books and thus are not introduced here.

4 Water Temperature

Water temperature is a key factor for water quality and ecological studies. It affects water chemistry such as gas solubility, chemical reactions, contaminant toxicity, and biological activities. It is influenced by heat fluxes across the water and bed surfaces, the temperature of upstream and lateral inflows, water depth, shading from river's bank landscape and vegetation, time of year, and latitude of the river.

The water temperature model describes heat transfer in the water column based on the first law of thermodynamics. The 1-D transport equation (3.1) can be applied here, with $S = q_T/(h\rho c_p)$, in which q_T is the net heat flux, ρ is the water density, h is the water depth, and c_p is the specific heat capacity. The net heat flux is considered as the exchange of heat across the air–water interface and the subsequent distribution of heat source throughout the water column. The surface heat flux consists of four major components: solar radiation (q_{sw}), long-wave atmospheric radiation (q_{lw}), latent heat flux (q_l), and convective heat flux (q_s), shown in Fig. 3.2. The

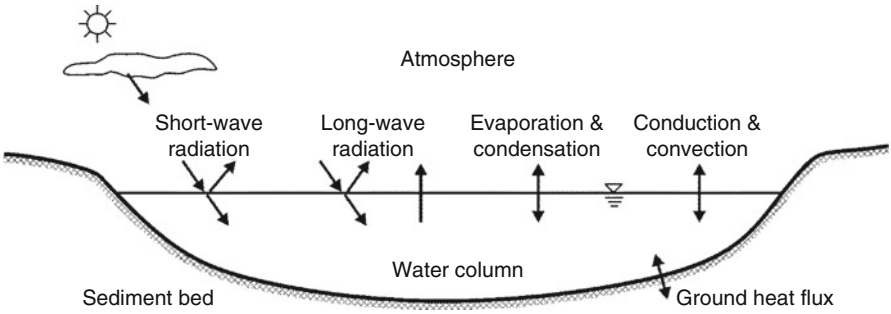

Fig. 3.2 Heat budget in water column

Table 3.1 Cloud cover and reflection coefficients [18]

Cloud cover	Overcast	Broken	Scattered	Clear
C_L	1.0	0.5–0.9	0.1–0.5	0
A	0.33	0.95	2.20	1.18
B	−0.45	−0.75	−0.97	−0.77

heat exchange with the underlying sediment is not considered in the present model, but can be readily added in the source/sink term q_T using methods presented in cited references such as [24]. The net heat flux is calculated as

$$q_T = q_{sw} + q_{lw} + q_l + q_s \tag{3.8}$$

The solar radiation is either measured directly or computed from a number of available formulas. It is a function of geographical location, time of year, hour of day, and cloudiness. The net solar radiation can be determined by [25, 26]

$$q_{sw} = q_{sw,clear}\left(1 - 0.65C_L^2\right)(1 - R_{sw})(1 - f_{shade}) \tag{3.9}$$

where

$q_{sw,clear}$ = short-wave radiation reaching the water surface on a clear day after atmospheric attenuation
C_L = fraction of cloud cover as given in Table 3.1
R_{sw} = albedo or reflection coefficient
f_{shade} = shading factor defined as the fraction of potential solar radiation that is blocked due to riparian vegetation and landscape.

Clouds have the greatest effect in reducing the amount of radiation energy received on the Earth [27]. The attenuation of solar radiation by clouds is difficult to predict due to a variety of types, distributions, and albedos of clouds. The reflection coefficient is calculated by [25, 26]

$$R_{sw} = A\left(\frac{180}{\pi}\alpha\right)^{B} \tag{3.10}$$

where

A and B = coefficients depending on the cloud cover as given in Table 3.1
α = altitude of the Sun in radians.

The long-wave or thermal radiation is radiation emitted by terrestrial object and the earth's atmosphere. The long-wave radiation depends on the surface temperature of the emitting object, air temperature, and water temperature. It is computed from the empirical formula of an overall atmospheric emissivity and the Stefan–Boltzmann law. The net long-wave radiation is determined by

$$q_{lw} = \varepsilon_{air}\sigma T_{air}^4\left(1 + 0.17C_L^2\right)(1 - R_{lw}) - \varepsilon_{water}\sigma T_{water}^4 \tag{3.11}$$

where

ε_{air} = emissivity value of air (= 0.96 for an approximation for normal and hemispherical emissivity)
ε_{water} = emissivity value of water ($= 0.938 \times 10^{-5}\ T^2_{air}$)
σ = Stefan–Boltzmann constant ($= 5.669 \times 10^{-8}$ W/m^2 °K^4)
T_{air} = air temperature, °K
T_{water} = surface water temperature, °K
R_{lw} = reflectivity of water surface for long-wave radiation (= 0.03).

The latent heat flux is a gain or loss of energy during a change in the state of water between liquid and vapor. The latent heat flux in natural water depends on vapor pressure, air temperature, wind speed, and dew point temperature. It is calculated as

$$q_l = f(U_w)(e_{air} - e_s) \tag{3.12}$$

where

$f(U_w)$ = function of wind speed, W/m^2 mb, as given in Table 3.2
e_{air} = air vapor pressure, mb
e_s = saturation vapor pressure, mb.

Table 3.2 Wind speed functions in W/m^2 mb [18]

Wind speed function formula[a]	$f(U_w)$
Meyer (1928)	$4.18 \times 10^{-9} + 0.95 \times 10^{-9}\ U_w$
Marciano and Harbeck (1952)	$1.02 \times 10^{-9}\ U_w$
Harbeck et al. (1959)	$1.51 \times 10^{-9}\ U_w$
Morton (1965)	$3.59 \times 10^{-9} + 1.26 \times 10^{-9}\ U_w$
Ryan and Harleman (1973)	$2.83 \times 10^{-9} + 1.26 \times 10^{-9}\ U_w$

[a]U_w is the wind speeds (m/s), typically specified as measured at a height of 2 m over the water surface

The saturation vapor pressure is the highest pressure of water vapor that can exist in equilibrium with a plane, free water surface at a given temperature. It is approximated by the Tetens formula as [26]

$$e_s = 6.108\exp\left(\frac{17.27T_{water}}{T_{water}+273.3}\right) \tag{3.13}$$

where

T_{water} = water temperature, °C.

The air vapor pressure, e_{air}, is calculated in a similar way by substituting T_{water} in Eq. (3.13) with the dew point temperature.

The convective or sensible heat is described as the heat flux transferred between air and water by conduction and transported away from/or toward the air–water interface. The amount of heat gained or lost through the sensible heat depends on the gradient of temperature in the vertical direction. The Bowen ratio describes the relationship between heat and vapor transport. The surface heat conduction is related to the evaporative heat flux and the Bowen ratio. It is estimated by [26]

$$q_s = c_b f(U_w)(T_{air} - T_{water}) \tag{3.14}$$

where

c_b = Bowen coefficient (=0.62 mb).

5 Kinetic Relations of Water Quality

The relationships of constituents in the developed water quality model are illustrated in Fig. 3.3. Nutrients and other constituents move in circular paths through biotic and abiotic components, which are known as biogeochemical cycles [28]. In the water column, four biogeochemical cycles are considered: oxygen, carbon, nitrogen, and phosphorus cycles.

Dissolved oxygen (DO) plays an important role in aquatic ecosystems. It is essential for living organisms and controls many chemical and biological reactions. Oxygen can be removed from or added to water by various physical, chemical, and biological processes. It is governed by

$$\frac{DC_{DO}}{Dt} = \left(\frac{32}{12}+\frac{48}{14}\alpha_{NC}\left(1-p_{NH_3}\right)\right)K_{ag}C_a - \frac{32}{12}\sum_{i\in\{a,z,f,p\}}K_{ir}C_i + K_{RE}\theta_{RE}^{T-20}\left(C'_{DO}-C_{DO}\right)$$
$$-K_{CBOD}\frac{C_{DO}}{h_{CBOD}+C_{DO}}\theta_{CBOD}^{T-20}C_{CBOD} - \frac{64}{14}K_{NH_3}\frac{C_{DO}}{h_{NH_3}+C_{DO}}\theta_{NH_3}^{T-20}C_{NH_3} + \frac{S_{SOD}}{h} \tag{3.15}$$

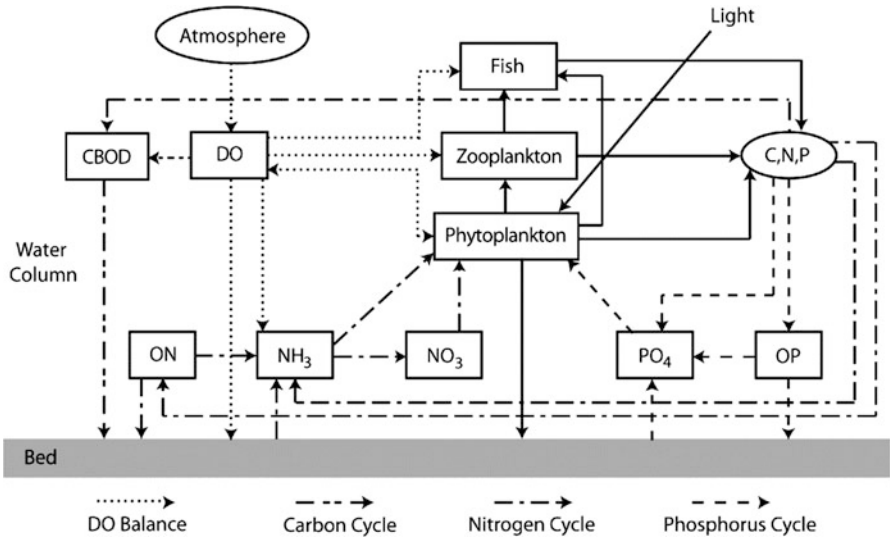

Fig. 3.3 Kinetic processes in water column

where

C_{DO} = DO concentration, g/m^3
C'_{DO} = saturation DO concentration, g/m^3
C_{NH3} = concentration of ammonia nitrogen, g/m^3
C_{CBOD} = concentration of carbonaceous biological oxygen demand (CBOD), g/m^3
C_a = biomass concentration of phytoplankton, g/m^3
C_i = biomass concentration of biotic organism i, g/m^3
i = organism index which specifies a as phytoplankton, z as zooplankton, f as forage fish, and p as predatory fish
K_{ag} = photosynthesis rate of phytoplankton, 1/d
K_{ir} = respiration rate of biotic organism i, 1/d
K_{RE} = depth-averaged reaeration rate, 1/d
K_{CBOD} = CBOD decay rate, 1/d
K_{NH3} = nitrification rate, 1/d
α_{NC} = stoichiometric ratio of nitrogen to carbon, gN/gC
p_{NH3} = ammonia preference factor, from Eq. (3.21)
h_{CBOD} = half-saturation DO concentration for CBOD decay, g/m^3
h_{NH3} = half-saturation DO concentration for nitrification, g/m^3
S_{SOD} = sediment oxygen demand flux, g/m^2 s
T = water temperature, °C
θ = temperature coefficient
h = water depth, m.

The saturation DO concentration is calculated as

$$C'_{DO} = \exp\left[c_0 + c_1/T_K + c_2/T_K^2 + c_3/T_K^3 + c_4/T_K^4\right] \tag{3.16}$$

where

$c_0 = -139.3441$
$c_1 = 1.5757 \times 10^5$
$c_2 = -6.6423 \times 10^7$
$c_3 = 1.2438 \times 10^{10}$
$c_4 = -8.6219 \times 10^{11}$
T_K = water temperature in °K ($T_K = T + 273.15$).

The reaeration rate K_{RE} in natural rivers depends on several factors, such as internal mixing and turbulence, temperature, wind speed, and water depth. Therefore, K_{RE} is given as a temporally and spatially varying rate which can be calculated from several existing formulas [29, 30], such as O'Connor–Dobbins (1958), Churchill (1962), Owen and Gibbs (1964), and Langbein and Durum (1967). These formulas adopt different functions of flow velocity and water depth for K_{RE}. Each formula was developed for certain hydrodynamic and topographic conditions and thus is adequate in different types of rivers. The Churchill formula is used in the test cases of the present study.

Sediment oxygen demand (SOD) is the rate at which dissolved oxygen is removed from the overlying water column by biological processes in the river bed sediments. SOD rate is mainly affected by biological factors such as organic content of the benthic sediment and microbial concentrations [31]. The sediment oxygen demand flux (S_{SOD}) is treated in the present model as input from measurement data. The flux can be given as a constant but mostly a spatially varying or spatially and temporally varying flux depending upon the availability of the data.

Biological oxygen demand (BOD) is one of the common water quality indicators. It is a measure of the amount of oxygen required to stabilize organic matter in the water. BOD_5 is determined from a standardized test, which measures the amount of oxygen available after incubation of the sample at 20 °C for a specific length of time, usually 5 days. The BOD kinetic processes are represented by the BOD formation, carbonaceous deoxygenation, nitrogenous deoxygenation, and BOD settling. Carbonaceous biological oxygen demand (CBOD) testing is similar to BOD testing with the exception that a nitrification inhibitor is added at the start of the process to eliminate nitrifying bacteria from water sample. Therefore only the carbonaceous demand is measured. The rate of change in CBOD concentration is determined as

$$\begin{aligned}\frac{DC_{CBOD}}{Dt} = {} & \frac{32}{12}K_{am}C_a + \frac{32}{12}\sum_{i\in\{z,f,p\}}(K_{im} + K_{ie} + K_{id})C_i - K_{CBOD}\frac{C_{DO}}{h_{CBOD} + C_{DO}}\theta_{CBOD}^{T-20}C_{CBOD} \\ & - \frac{5}{4}\frac{32}{14}K_{NO_3}\frac{h_{NO_3}}{h_{NO_3} + C_{DO}}\theta_{NO_3}^{T-20}C_{NO_3} + \frac{\omega_{CBOD}}{h}f_{PBOD}C_{CBOD}\end{aligned} \tag{3.17}$$

where

C_{NO3} = concentration of nitrate nitrogen, g/m^3
K_{im} = mortality rate of biotic organism i, 1/d
K_{ie} = excretion rate of biotic organism i, 1/d
K_{id} = defecation rate of biotic organism i, 1/d
K_{NO3} = denitrification rate, 1/d
h_{NO3} = half-saturation DO concentration for denitrification, g/m^3
ω_{CBOD} = settling velocity of CBOD, m/s
f_{PBOD} = fraction of particulate CBOD in total CBOD.

The major components of nitrogen in aquatic ecosystems are organic nitrogen (ON), ammonia (NH_3), and nitrate (NO_3). Mortality of biotic organisms produces organic nitrogen, which is converted into ammonia through bacteria decomposition. In the presence of nitrifying bacteria and oxygen, ammonia is oxidized to nitrite (NO_2) and nitrate via nitrification. The uptake of ammonia and nitrate by plants is through the assimilation process. In natural water, the presence of nitrogen gives rise to nitrification problem, eutrophication, and ammonia toxicity [29]. Nitrification reduces the oxygen level. One of the byproducts of nitrification is nitrate, which is a pollutant. Depending on the pH and temperature, ammonia can manifest itself into an un-ionized form, which is toxic to aquatic organisms. Both ammonia and nitrate are essential nutrients for photosynthesis, but high levels of ammonia and nitrate can result in excessive phytoplankton growth and in turn water quality problems. The kinetic processes of nitrogen are described by the following equations:

$$\frac{DC_{ON}}{Dt} = \sum_{i\in\{a,z,f,p\}} \left(1 - f_{NH_3}\right) K_{im}\alpha_{NC}C_i - K_{ON}\frac{C_a}{h_{ON} + C_a}\theta_{ON}^{T-20}C_{ON} - \frac{\omega_{ON}}{h}f_{PON}C_{ON} + \frac{S_{ON}}{h} \tag{3.18}$$

$$\frac{DC_{NH_3}}{Dt} = \sum_{i\in\{a,z,f,p\}} f_{NH_3}K_{im}\alpha_{NC}C_i + \sum_{i\in\{z,f,p\}} K_{ie}\alpha_{NC}C_i + K_{ON}\frac{C_a}{h_{ON} + C_a}\theta_{ON}^{T-20}C_{ON} - K_{ag}p_{NH_3}\alpha_{NC}C_a - K_{NH_3}\frac{C_{DO}}{h_{NH_3} + C_{DO}}\theta_{NH_3}^{T-20}C_{NH_3} + \frac{S_{NH_3}}{h} \tag{3.19}$$

$$\frac{DC_{NO_3}}{Dt} = K_{NH_3}\frac{C_{DO}}{h_{NH_3} + C_{DO}}\theta_{NH_3}^{T-20}C_{NH_3} - K_{ag}\left(1 - p_{NH_3}\right)\alpha_{NC}C_a - K_{NO_3}\frac{h_{NO_3}}{h_{NO_3} + C_{DO}}\theta_{NO_3}^{T-20}C_{NO_3} + \frac{S_{NO_3}}{h} \tag{3.20}$$

where

C_{ON} = concentration of organic nitrogen, g/m^3
K_{ON} = mineralization rate of organic nitrogen, 1/d
f_{NH3} = fraction of ammonia in dead organic material
ω_{ON} = settling velocity of organic nitrogen, m/s
f_{PON} = fraction of particulate organic nitrogen to organic nitrogen
S = concentration flux from the sediment bed, g/m^{2}s.

The ammonia preference factor is introduced to take into account the preference of ammonia over nitrate when both are available for phytoplankton to uptake, and calculated by

$$p_{NH_3} = \frac{C_{NH_3}C_{NO_3}}{(h_N + C_{NH_3})(h_N + C_{NO_3})} + \frac{C_{NH_3}h_N}{(C_{NH_3} + C_{NO_3})(h_N + C_{NO_3})} \tag{3.21}$$

where

h_N = Michaelis–Menten constant for nitrogen uptake, mgN/L.

Phosphorus in natural water exists in several states. The soluble reactive phosphorus (SRP), also called orthophosphate or soluble inorganic phosphorus, is the form that is readily available to phytoplankton. Particulate organic phosphorus is the form that mainly stays with living plants, animals, bacteria, and organic detritus. Nonparticulate organic phosphorus can be dissolved or colloidal organic compounds containing phosphorus. They are usually from the decomposition of particulate organic phosphorus. Particulate inorganic phosphorus consists of phosphate mineral, sorbed orthophosphate, and phosphate complex with solid matter. Nonparticulate inorganic phosphorus includes condensed phosphate such as those found in detergents. In the present model, phosphorus is divided into two main groups: organic phosphorus (OP) and inorganic phosphorus (orthophosphate, PO_4). The kinetic processes of phosphorus are governed by

$$\frac{DC_{OP}}{Dt} = \sum_{i\in\{a,z,f,p\}} (1 - f_{PO_4})K_{im}\alpha_{PC}C_i - K_{OP}\frac{C_a}{h_{OP} + C_a}\theta_{OP}^{T-20}C_{OP} - \frac{\omega_{OP}}{h}f_{POP}C_{OP} + \frac{S_{OP}}{h} \tag{3.22}$$

$$\frac{DC_{PO_4}}{Dt} = \sum_{i\in\{a,z,f,p\}} f_{PO_4}K_{im}\alpha_{PC}C_i + \sum_{i\in\{z,f,p\}} K_{ie}\alpha_{PC}C_i + K_{OP}\frac{C_a}{h_{OP} + C_a}\theta_{OP}^{T-20}C_{OP} - K_{ag}\alpha_{PC}C_a + \frac{S_{PO_4}}{h} \tag{3.23}$$

where

C_{OP} = concentration of organic phosphorus, g/m^3
C_{PO4} = concentration of orthophosphate, g/m^3

α_{PC} = stoichiometric ratio of phosphorus to carbon, gP/gC
K_{OP} = mineralization rate of organic phosphorus, 1/d
h_{OP} = half-saturation phytoplankton conc. for mineralization of phosphorus, mg/L
ω_{OP} = settling velocity of organic phosphorus, m/s
f_{POP} = fraction of particulate organic phosphorus to organic phosphorus
f_{PO4} = fraction of phosphate in dead organic material.

6 Food Web Relations

The food webs in river systems are quite complex, and modeling of food web dynamics coupled with the water quality model is usually case-dependent. Therefore, several assumptions are made in order to simplify prey–predator relationships. Firstly, biotic organisms are considered separately as groups according to trophic levels. The upper trophic level can feed on the lower level as its food. Secondly, the feeding preference of predator on a particular group of prey is the same regardless of size, density, and distribution of prey. However, the feeding preference can be different when predator feeds on different groups of prey. Finally, age-structure is not considered in the model, and consequently the kinetic rates such as grazing and respiration rates of each group are given as constants.

In this study, the food web model consists of four trophic levels: phytoplankton, zooplankton, forage fish, and predatory fish, and phytoplankton is assumed to be the lowest trophic level or the main food source of the upper trophic levels. Certainly this assumption has limitation because some stream ecosystems are also based on insects, benthic fauna, and benthic algae, which are not included here.

The dynamic processes of phytoplankton are described by

$$\frac{DC_a}{Dt} = \left(K_{ag} - K_{ar} - K_{ae} - K_{am}\right)C_a - \sum_{i\in\{z,f,p\}} K_{ig} f_{ai} C_i - \frac{\omega_a}{h} C_a \tag{3.24}$$

where

K_{ag} = rate of photosynthesis, 1/d
K_{ar} = rate of respiration of phytoplankton, 1/d
K_{ae} = rate of excretion of phytoplankton, 1/d
K_{am} = rate of nonpredatory mortality of phytoplankton, 1/d
K_{ig} = grazing rate of predator i (= z, f, p), 1/d
f_{ai} = relative preference of predator i on phytoplankton as food
ω_a = settling velocity of phytoplankton, m/d.

The photosynthesis rate is modeled as the maximum photosynthesis rate ($K_{ag,max}$) multiplied by environmental factors as

$$K_{ag} = K_{ag,\max} f_N f_L f_T f_{TOX} \tag{3.25}$$

where

f_N = nutrient limitation factor
f_L = light limitation factor
f_T = temperature limitation factor
f_{TOX} = reduction factor due to toxic chemical from Eq. (3.57).

The nutrient limitation factor for photosynthesis process is computed using a Michaelis–Menten equation as follows [32]

$$f_N = \min\left(\frac{C_{NH_3} + C_{NO_3}}{h_N + C_{NH_3} + C_{NO_3}}, \frac{C_{PO_4}}{h_P + C_{PO_4}}\right) \tag{3.26}$$

where

h_N = half-saturation concentration for nitrogen, g/m^3
h_P = half-saturation concentration for phosphorus, g/m^3.

The effect of light on phytoplankton growth is complex. The interception and utilization of light by phytoplankton determine net productivity, species succession, and abundance of higher trophic organisms [33]. Several factors, such as the light attenuation through water depth and the dependence of growth on light, can be integrated to come up with the total effect. The depth-averaged light limitation factor is modeled as [34]

$$f_L = \frac{1}{\gamma h} \ln\left(\frac{h_L + I_0}{h_L + I_0 e^{-\gamma h}}\right) \tag{3.27}$$

where

I_0 = light intensity at the water surface
h_L = half-saturation light intensity for phytoplankton growth
γ = light extinction, 1/m.

The light extinction is calculated by the modified equation from the WASP6 model as [6]

$$\gamma = \gamma_0 + 0.0088C_a + 0.054C_a^{0.67} + 0.0458C_m \tag{3.28}$$

where

γ_0 = background light extinction, 1/m
C_a = phytoplankton concentration as total Chlorophyll-a, μg/L
C_m = concentration of suspended solid, g/m^3.

Aquatic organisms have preferred temperature ranges. Biological production increases as a function of temperature until an optimum temperature. The temperature limitation factor for biological growth is calculated using the Cerco and Cole's formula as [5]

$$f_T = \begin{cases} \exp\left[-KT_{g1}\left(T - T_{opt}\right)^2\right] & T \le T_{opt} \\ \exp\left[-KT_{g2}\left(T_{opt} - T\right)^2\right] & T > T_{opt} \end{cases} \tag{3.29}$$

where

T_{opt} = optimal temperature for biological growth
KT_{g1} = coefficient representing the relationships of growth on temperature below the optimal temperature
KT_{g2} = coefficient representing the relationships of growth on temperature above the optimal temperature.

Compared to the theta model described below, the Cerco and Cole's formulation may become necessary when several individual species or groups of algae are modeled because each group of algae is sensitive to temperature differently [29].

For respiration, excretion, and non-predatory mortality rates of phytoplankton, the temperature limitations are computed by the theta model, $f_T = \theta^{T-20}$, as follows:

$$K_{ar} = K_{ar,\max}\theta_a^{T-20} \tag{3.30}$$

$$K_{ae} = K_{ae,\max}\theta_a^{T-20} \tag{3.31}$$

$$K_{am} = \left(1 + f'_{am}\right)K_{am,\max}\theta_a^{T-20} \tag{3.32}$$

where

$K_{ar,max}$ = maximum rate of respiration of phytoplankton, 1/d
$K_{ae,max}$ = maximum rate of excretion of phytoplankton, 1/d
$K_{am,max}$ = maximum rate of nonpredatory mortality of phytoplankton, 1/d
f'_{am} = increase factor in the mortality due to toxic chemicals which can be calculated from the general form shown in Eq. (3.55).

For a higher trophic level (i = z, f, p), the dynamic process is modeled as

$$\frac{DC_i}{Dt} = \left(K_{ig} - K_{ir} - K_{ie} - K_{im} - K_{id} - K_{ib} + K_{ire}\right)C_i - \sum\nolimits_j K_{jg} f_{ij} C_j \tag{3.33}$$

where

K_{ig} = grazing rate of organism i, 1/d
K_{ir} = respiration rate of organism i, 1/d
K_{ie} = excretion rate of organism i, 1/d
K_{im} = nonpredatory mortality rate of organism i, 1/d
K_{id} = defecation rate of organism i, 1/d
K_{ib} = gamete loss rate of organism i, 1/d

K_{ire} = reproduction rate of organism i, 1/d
f_{ij} = relative preference factor of predator j feeding on organism i as food.

The general formulation of the grazing rate is computed by

$$K_{ig} = K_{ig,\max}\lambda_i f_T f'_{ig} \tag{3.34}$$

where

$K_{ig,max}$ = maximum grazing rate of predator i, 1/d
λ_i = grazing limitation factor
f_T = temperature limitation factor from Eq. (3.29)
f'_{ig} = reduction factor in animal growth due to toxic chemical from Eq. (3.58).

The maximum grazing rate can be given as a constant, but it is generally calculated from the body weight with $K_{ig,max} = a_i W_i^{bi}$, where a_i is the weight specific consumption, b_i is the slope of the allometric function, and W_i is the average body weight of organism i.

The grazing limitation factor λ_i reduces the grazing rate of predator when food concentrations are low. λ_i is calculated by using a modified Michaelis–Menten factor and a threshold food concentration μ_j, which is revised from the equation of Rounds et al. [35]:

$$\lambda_i = \frac{\sum_j (p_{ji}C_j - \mu_j)}{h_i + \sum_j (p_{ji}C_j)} \tag{3.35}$$

where

h_i = half-saturation food concentration for grazing, g/m^3
p_{ji} = preference of predator i feeding on organism j as food.

The general form of relative preference of predator i on organism j as food, used in the grazing term of each prey–predator relationship, is calculated as $f_{ji} = p_{ji}C_i / \sum_j (p_{ji}C_i)$ [10].

It should be noted that detritus, which is derived from the mortality, excretion, and defecation of living organisms, can be a food source for zooplankton and fish and thus is considered in the present food web model. However, the concentration of detritus, C_d, is not computed directly, but related to the CBOD by a simple relation: $C_d = 12/32 \times C_{CBOD}$.

The excretion and non-predatory mortality rates of zooplankton and fish are modeled as single first-order kinetics similar to the phytoplankton model:

$$K_{ie} = K_{ie,\max}\theta_i^{T-20} \tag{3.36}$$

$$K_{im} = \left(1 + f'_{im}\right)K_{im,\max}\theta_i^{T-20} \tag{3.37}$$

where

$K_{ie,max}$ = maximum rate of excretion of organism i, 1/d
$K_{im,max}$ = maximum rate of nonpredatory mortality of organism i, 1/d
f'_{im} = increase factor in the mortality due to toxic chemicals from Eq. (3.55).

A fraction of ingested food can be egested as feces or discarded as organic material. The defecation rate of unassimilated food depends on the assimilating efficiency e_{ig} and is determined as

$$K_{id} = \left(1 - e_{ig}\right) f'_{id} K_{ig} \tag{3.38}$$

where

f'_{id} = increase factor in the defecation due to toxic chemicals from Eq. (3.59).

The respiration of zooplankton and fish can be modeled as single first-order kinetics with a rate as

$$K_{ir} = K_{ir,\max} \theta_i^{T-20} \tag{3.39}$$

where

$K_{ir,max}$ = maximum respiration rate of organism i, 1/d.

The respiration in fish is comprised of three components: standard, active, and dynamic respirations. Standard respiration is a rate at resting in which the organism is expending energy without consumption. Active respiration depends on swimming speed and temperature. The dynamic action is the metabolic action due to digesting and assimilating prey. The maximum respiratory rate of fish (i = f, p) can be calculated as [10]

$$K_{ir,\max} = K_{ir0} f_{den} f_{act} + f_{dyn}\left(K_{ig} e_{ig} - K_{id}\right) \tag{3.40}$$

where

K_{ir0} = basal or standard respiratory rate, 1/d
f_{act} = factor for respiratory rate associated with swimming or active respiratory fraction
f_{dyn} = proportion of assimilated energy lost to specific dynamic action
f_{den} = density-dependent respiration factor and can be computed by [10, 36]

$$f_{den} = 1 + 0.25 C_i / K_i \tag{3.41}$$

where
C_i = biomass concentration of fish i, g/m^3
K_i = carrying capacity of fish i, g/m^3 which depends on species and location. In this study, the carrying capacity value is taken from [10, 37].

The gamete and reproduction rates are only used in fish dynamic models. Eggs and sperm (gametes) in adult fish are a significant fraction of fish biomass. The

production of gametes is influenced by environmental factors, such as temperature, genetic factors, hormones, and nutrition. Gametogenesis and spawning occurs during a defined period when the environmental conditions are optimal in terms of survival. It is assumed that spawning occurs when the water temperature enters an appropriate range of optimal temperature which is between $0.6T_{opt}$ and $T_{opt} - 1$, where T_{opt} is the optimal water temperature for fish spawning [10]. This gamete loss can be determined by

$$K_{ib} = K_{ib0}\left(1 + f'_{ib}\right)\min(1, C_i/K_i) \tag{3.42}$$

where

K_{ib0} = intrinsic gamete mortality rate, 1/d
f'_{ib} = increase factor in the gamete due to toxic chemicals from Eq. (3.60).

In general, only a fraction of the gametes results in the biomass of young fish and subsequently adult fish. Some of them unsuccessfully reproduce and become organic materials. The increase in the biomass of small fish due to spawning in large fish when both are in the same species is referred to as reproduction. There are many environmental factors resulting in reproduction failure such as predator and toxic chemical. Due to the uncertainty of the reproduction process, these factors are neglected in this study. For the simplified single-age structure of fish dynamics, the reproduction rate K_{ire} depends on the gamete loss in adult fish, the percentage of success in reproduction, r_{ire}, and the biomass ratio between young-of-the-year (YOY) fish and adult fish, r_{iYA}, for a given fish species, as expressed with $K_{ire} = K_{ib0}\min(1, C_i/K_i)r_{ire}r_{iYA}$.

7 Fate and Transport of Contaminants

When a contaminant is discharged into a river, it is subject to fate and transport processes as shown in Fig. 3.4. It is usually dissolved in the water or absorbed by the moving sediments. Changes in concentration of the contaminant in the water column are caused by advection, diffusion (mixing), external loading, sorption, desorption, volatilization, photolysis, microbial decay, settling with sediments, exchange with the bed, uptake and depuration by the aquatic organisms, etc. One may determine the dissolved and absorbed contaminants separately using the non-equilibrium partition model or the total concentration by assuming the dissolved and absorbed phases in the equilibrium state [24]. The latter approach is used here, so that the contaminant transport in the water column is governed by Eq. (3.1) with the source/sink terms:

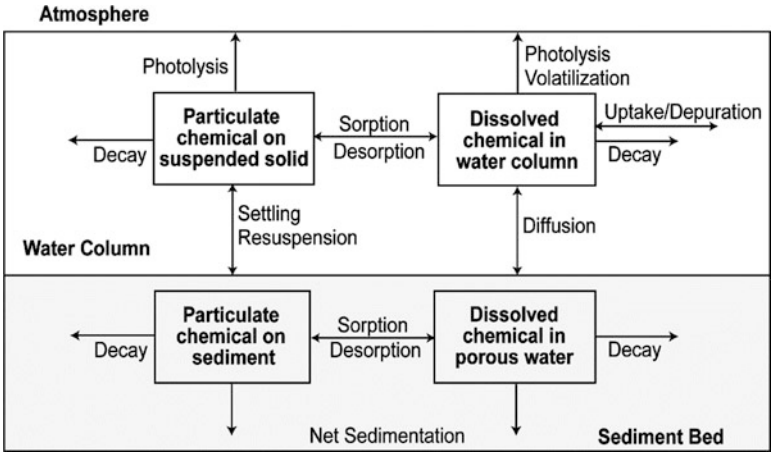

Fig. 3.4 Fate and transport of contaminants in water column and sediment bed

$$\frac{DC_{tw}}{Dt} = q_{tw} + \frac{J_{dbw}}{h} + \frac{q_{t,ex}}{h} - \left(K_N + K_H[H]^+ + K_{OH}[OH]^-\right) f_{dw} C_{tw} - K_p C_{tw} - K_b C_{tw}$$
$$-\frac{K_v}{h}\left(\frac{C_g}{H/RT_K} - f_{dw} C_{tw}\right) - K_{a1} f_{dw} C_{tw} C_a + K_{a2} C_{ta} - \sum_{j=\{z,f,p\}} \left(K_{j1} f_{dw} C_{tw} - K_{j2} C_{tj}\right) \tag{3.43}$$

where

C_{tw} = total concentration of contaminant in the water column, g/m^3
f_{dw} = fraction of dissolved concentration to the total concentration of contaminant in water column
q_{tw} = total loading rate of contaminant per unit volume, g/m^{3}d
J_{dbw} = vertical diffusion fluxes between water column and bed surface layer, g/m^{2}d
$q_{t,ex}$ = total exchange rate of contaminant due to sediment erosion and deposition, g/m^{2}d
K_N = neutral hydrolysis rate, 1/d
K_H = acid-catalyzed hydrolysis rate, m^3/mold
K_{OH} = base-catalyzed hydrolysis rate, m^3/mol d
$[H]^+$ = molar concentration of hydrogen ion, mol/m^3
$[OH]^-$ = molar concentration of hydroxide ion, mol/m^3
K_p = photolysis rate, 1/d
K_b = biodegradation rate, 1/d
K_v = volatilization rate, m/d
H = Henry's law constant, atm m^3/mol
R = universal gas constant, atm m^3/mol °K
C_g = gas-phase concentration of the contaminant, g/m^3.

Note that the last three terms in Eq. (3.43) are related to the changes in contaminant concentrations due to biotic organisms, and the related variables and explanations are given in Sect. 8.

The flux between the bed pore water and the water column occurs through diffusion at the interface, which is calculated using the Fick's law as

$$J_{dbw} = k_{dbw}\left(f_{db,1}C_{tb,1} - f_{dw}C_{tw}\right) \tag{3.44}$$

where

k_{dbw} = diffusional transfer coefficient of dissolved contaminant across the bed surface
$C_{tb,1}$ = total concentrations of contaminant in bed surface layer
$f_{db,1}$ = fraction of dissolved contaminant in bed surface layer.

By using the linear isotherm of sorption–desorption process, the fractions of dissolved and particulate contaminants in the water column and sediment bed are computed by [29]

$$f_{dw} = 1/(1 + K_d C_m), \quad f_{pw} = 1 - f_{dw} \tag{3.45}$$

$$f_{db} = \phi/(\phi + K_d \rho_d), \quad f_{pb} = 1 - f_{db} \tag{3.46}$$

where

f_{pw} = fraction of particulate contaminant in the water column
f_{pb} = fraction of particulate contaminant in the bed sediment
K_d = sorption–desorption coefficient, m^3/g
C_m = suspended sediment concentration, g/m^3
ϕ = porosity
ρ_d = dry density of the bed sediment, g/m^3.

The exchange rate of contaminant due to deposited and eroded sediments is calculated by [24]

$$q_{t,ex} = \max(E_b - D_b, 0)\frac{C_{tb,1}}{1-\phi} + \min(E_b - D_b, 0)\left(\frac{\phi}{1-\phi}\frac{f_{dw}C_{tw}}{1-m} + \frac{f_{pw}C_{tw}}{m}\right) \tag{3.47}$$

where

D_b = sediment deposition rate, m/d
E_b = sediment erosion rate, m/d
m = suspended sediment concentration by volume.

These sediment quantities in the above equation are computed in the sediment model. The first term on the right-hand side accounts for the net erosion case, with $1/(1-\phi)$ converting the net eroded bed sediment rate $\max(E_b - D_b, 0)$ to the net

erosion rate of the bed sediment and pore water mixture in which $C_{tb,1}$ is defined (contaminant mass over the total volume of the bed sediment and pore water mixture). Note that the pore water between the eroded sediment particles is also entrained into the water column. The second term on the right-hand side accounts for the net deposition case, in which the net deposited sediment rate is $\min(E_b - D_b, 0)$. This sediment is equivalent to a volume of $\min(E_b - D_b, 0)/m$ in the water column in which C_{tw} is defined. In the meantime, this net deposited sediment accompanies with water from the water column to bed pores, and the volume rate of this water is $\min(E_b - D_b,0)\ \phi/(1-\phi)$ in the bed surface layer, which is equivalent to a volume of $\min(E_b - D_b,0)\phi/[(1-\phi)(1-m)]$ in the water column in which C_{tw} is defined. Therefore, the second term on the right-hand side includes the contaminants dissolved in the water column and absorbed with moving sediment that both deposit onto the bed. Detailed derivation of Eq. (3.47) can be found in [24].

Contaminant in the sediment bed is usually transported by the pore water flow, and the thin surface layer in the bed may be mixed by bioturbation. For simplicity, a vertical diffusion model is used in this study, which divides the sediment bed into a suitable number of layers (three layers are used here as example) and determines the fate and transport of contaminant in the bed layers as [24, 38]

$$\frac{\partial(\delta_1 C_{tb,1})}{\partial t} = Q_{tb,1} - k_{tb,1}\delta_1 C_{tb,1} - k_{dbw}\left(f_{db,1}C_{tb,1} - f_{dw}C_{tw}\right) - q_{t,ex} + k_{db12}\left(f_{db,2}C_{tb,2} - f_{db,1}C_{tb,1}\right) + q_{tb12} \tag{3.48}$$

$$\frac{\partial(\delta_2 C_{tb,2})}{\partial t} = Q_{tb,2} - k_{tb,2}\delta_2 C_{tb,2} - k_{db12}\left(f_{db,2}C_{tb,2} - f_{db,1}C_{tb,1}\right) - q_{tb12} + k_{db23}\left(f_{db,3}C_{tb,3} - f_{db,2}C_{tb,2}\right) \tag{3.49}$$

$$\frac{\partial(\delta_3 C_{tb,3})}{\partial t} = Q_{tb,3} - k_{tb,3}\delta_3 C_{tb,3} - k_{db23}\left(f_{db,3}C_{tb,3} - f_{db,2}C_{tb,2}\right) \tag{3.50}$$

where

$C_{tb,i}$ = total concentration of contaminant in bed layer i
δ_i = thickness of layer i
$Q_{tb,i}$ = total contaminant loading rate in layer i
$k_{tb,i}$ = decay coefficient of contaminant at layer i
$k_{dbi,i+1}$ = diffusional transfer coefficient of dissolved contaminant between layers i and i + 1
$q_{tbi,i+1}$ = total exchange rate of contaminant between layers i and i + 1 due to lowering and rising of the interface.

Note that it is assumed in Eqs. (3.48)–(3.50) that the interface between bed layers 1 and 2 may lower or rise due to bed change, while the interface between bed layers 2 and 3 does not change, as explained in [22].

8 Bioaccumulation Processes

The transfers of contaminant in water through surface sorption of phytoplankton and gill and dietary uptakes in fish are important routes of contaminant uptake in aquatic ecosystems. The contaminant concentration in the aquatic organisms is governed by the advection–dispersion equation as shown in Eq. (3.1). The dynamic processes for contaminant concentration in phytoplankton can be described by a simple linear reversible sorption–desorption equation suggested in [39]. The resulting net source term in Eq. (3.1) is [10]

$$\frac{DC_{ta}}{Dt} = K_{a1} f_{dw} C_{tw} C_a - K_{a2} C_{ta} - (K_{ae} + K_{am}) C_{ta} - \sum_{i \in \{z,f,p\}} \left(K_{ig} f_{ai} C_i\right) \nu_a \quad (3.51)$$

where

C_{ta} = concentration of contaminant associated with phytoplankton in unit volume of water column, g/m^3
K_{a1} = uptake rate of contaminant, m^3/g d
K_{a2} = depuration rate of contaminant, 1/d
ν_a = concentration of contaminant in phytoplankton, g/g.

The concentration of contaminant in organism i is calculated by

$$\nu_i = C_{ti}/C_i \quad (3.52)$$

where

C_{ti} = contaminant concentration associated with organism i in unit volume of water column, g/m^3
C_i = biomass concentration of organism i, g/m^3.

For higher trophic levels, the input of contaminant due to ingestion of contaminated food plays an important role. The rate of change in contaminant concentration in biotic organism i (=z, f, p) is determined by

$$\frac{DC_{ti}}{Dt} = K_{i1} f_{dw} C_{tw} + \sum\nolimits_k K_{ig} e_{ig} C_i f_{ki} v_k - (K_{i2} + K_{im} + K_{id} + K_{ib}) C_{ti} - \sum\nolimits_j \left(f_{ij} K_{jg} C_j\right) \nu_i \quad (3.53)$$

where

K_{i1} = uptake rate of contaminant of organism i, 1/d
K_{i2} = depuration rate of contaminant of organism i, 1/d
j = organism index representing predator of organism i
k = organism index representing prey of organism i.

Connolly et al. [40] proposed a formula to determine the uptake rate of contaminant by an aquatic organism. The uptake rate depends on the respiration rate and transfer efficiency across the organism's membrane. The depuration of contaminant is related to the characteristics of organism such as body weight and lipid content and the chemical properties of the contaminant, i.e., the octanol–water partition coefficient, K_{ow} [10]. Due to a single-age class of the current fish dynamic model, body weight and lipid content are kept as constants. Therefore, the uptake and depuration rates of contaminant cannot be determined from the existing formula. They are treated as calibrated constant parameters, similar to the other kinetics rates in the fish model, for instance, grazing and respiration rates.

9 Effects of Toxic Chemicals

Biomass loss due to acute toxicity is estimated based on the internal concentration of the contaminant in the biotic organism, IC_{i50}. The internal concentration depends on the concentration of contaminant in water that causes 50 % mortality for a given period of exposure, LC_{i50}, and the bioconcentration factor, BCF, where $IC_{i50} = LC_{i50} \times BCF$. The constant uptake and depuration rates of contaminant are used, thus the constant BCF is applied for all aquatic organisms in the current model. The internal concentrations of contaminant vary due to the depuration process of organisms. The time-varying concentration of the contaminant C_{i50} is calculated as [10]

$$C_{i50} = IC_{i50}\left(1 - e^{-K_{i2}\, t_1}\right)/\left(1 - e^{-K_{i2}\, t_2}\right) \tag{3.54}$$

where

t_1 = exposure time in toxicity test
t_2 = period of exposure.

The fraction killed by a given internal concentration of toxicant is estimated using the time-dependent C_{i50} in the cumulative form that is determined by [10]

$$f'_{im} = 1 - \exp(-v_i/C_{i50})^{1/K_s} \tag{3.55}$$

where

f'_{im} = fraction of organism i killed for a given period of exposure
K_s = parameter representing toxic response (= 0.33).

When the concentration level of the contaminant is less than the level causing death, organisms still experience some adverse effects. The ratio of chronic to acute concentration is used to predict the chronic effect, and is calculated by

$$r_{i50} = EC_{i50}/LC_{i50} \tag{3.56}$$

where

r_{i50} = chronic to acute ratio
EC_{i50} = contaminant concentration in water that causes 50 % reduction in photosynthesis, growth, or reproduction.

The effects of contaminant on phytoplankton photosynthesis and animal growth and reproduction are considered through the reduction factor f_{TOX}. The general form is expressed as [10]:

$$f_{TOX} = \exp(-v_i/C_{i50}r_{i50})^{1/K_s} \tag{3.57}$$

For phytoplankton, the effect of chemical from Eq. (3.57) is directly applied into the photosynthesis rate of phytoplankton in Eq. (3.25). However, in animals, the reduction factor for growth is related to assimilation and defecation processes. It is assumed that 20 % of the assimilation is reduced while the amount of food that is not assimilated increases by 80 % [10]

$$f'_{ig} = 1 - 0.2f_{TOX} \tag{3.58}$$

$$f'_{id} = 1 + 0.8f_{TOX} \tag{3.59}$$

where

f'_{ig} = reduction factor for animal assimilation
f'_{id} = increase factor for the amount of unassimilated food.

The effect of contaminant on the reproduction of animals is complex since several factors are involved in the reproductive failure. For simplification, the reduction factor for reproduction is applied only for the increase of gamete mortality, which is written as

$$f'_{ib} = 1 - f_{TOX} \tag{3.60}$$

where

f'_{ib} = increase factor in gamete loss due to contaminant.

Note that f_{TOX} in Eq. (3.60) is calculated from Eqs. (3.56) and (3.57) by using the contaminant concentration in water that causes 50 % reduction in reproduction EC_{i50}.

10 Model Test

10.1 Model Test in the Tualatin River, Oregon

10.1.1 Study Area

The Tualatin River is located in the west side of the Portland metropolitan area, northwestern Oregon, USA. Its watershed drains 1844 km^2. The main stem of the river is approximately 128 km, originates in the Coast Range, and flows eastward before joining the Willamette River near West Linn, as shown in Fig. 3.5. The average slope and width of the river ranges 0.01524–14.1 m/km and 4.6–46 m, respectively [35]. Historically, the wastewater treatment plants in the urban area of the Tualatin River watershed discharged high concentrations of ammonia and phosphorus into the river [35]. The river at the lower reaches encountered algal blooms and consequently faced water quality problem. The water quality violations in the river included the minimum DO level, the maximum pH standard, and the exceedance of phytoplankton concentration.

Water quality and ecological properties of the Tualatin River in the period from May 1, 1991 to October 31, 1993 are simulated in this study. The simulation domain is approximately 50 km long, from the Rood Bridge at Hillsboro or at river mile (RM, 1 mile = 1.61 km) 38.4 to the Stafford Road near Lake Oswego (RM5.5). It is represented by 132 cross-sections, and each cross-section is divided into 11 vertical panels. The time step is 15 min. Several tributaries, irrigation withdrawals, and two wastewater treatment plants (WWTP) at Rock Creek (RM38.1) and Durham (RM9.3) are included as side discharges. The measurement data for hydrodynamic, water quality, and ecological properties are reported in [41], and the estimated irrigation withdrawals are published in [35]. Daily air temperature, dew point temperature, wind speed, wind direction, and precipitation (rainfall) measured at the Tualatin Valley Irrigation District (TVID) Agrimet Weather Station located in Verboort, Oregon [41] are used as inputs for water temperature simulation. Details on data interpretation and assumption are summarized in [42].

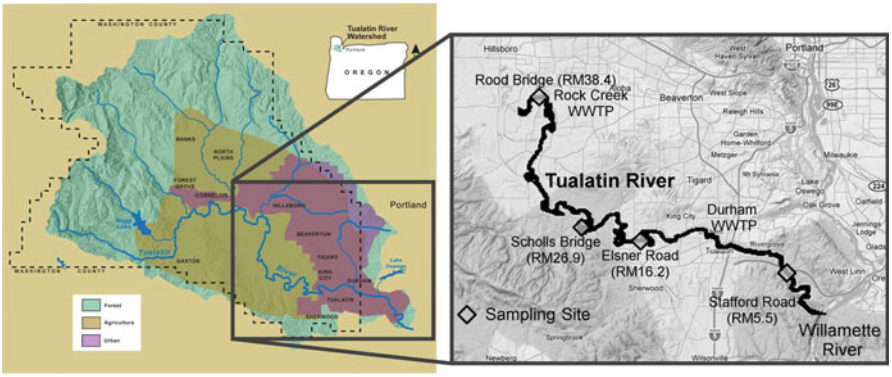

Fig. 3.5 Study domain: Tualatin River, Oregon (http://www.trwc.org and www.maps.google.com)

10.1.2 Estimation and Calibration of Model Parameters

Model parameters are important for determining the transport and transformation of each constituent in the model. Some parameters are taken from technical reports such as [35, 43, 44], and some are calibrated. For example, the Manning's roughness coefficient n is calibrated as a constant value of 0.025 $s/m^{1/3}$ in the entire simulation domain. The longitudinal dispersion coefficient D_x is calibrated as 5.0 m^2/s by simulating a conservative tracer, chloride. Selected parameters related to water quality and ecological simulations are given in Tables 3.3 and 3.4, respectively.

The zooplankton abundance may be affected by planktivory fish [35]. However, because there is no fish data available, the fish is not considered in this case. Therefore, the predatory and non-predatory mortality rates of zooplankton are combined as a single mortality rate, which is calibrated as 0.005 1/d. The zooplankton grazing rate coefficient is allowed to vary during the simulation period. It is calibrated as a constant value of 0.9 1/d in the reach upstream of RM12.25, and varies seasonally between 0.6 and 1.2 1/d in the reach downstream of RM12.25 as presented in Fig. 3.6. Such difference between the upstream and downstream reaches may reflect different biotic processes due to a large amount of organic materials accumulated at the river bed in downstream reaches [44].

Table 3.3 Summary of model parameters for water quality simulations

Symbol	Unit	Value	Symbol	Unit	Value
K_{ON}	1/d	0.20	f_{PO4}	–	0.75
K_{NH3}	1/d	0.05	f_{PBOD}	–	0.5
K_{NO3}	1/d	0.10	h_{NH3}	mg O_2/L	2.5
K_{OP}	1/d	0.25	h_{NO3}	mg O_2/L	2.0
K_{CBOD}	1/d	0.25	h_{CBOD}	mg O_2/L	0.5
α_{NC}	gN/gC	0.16	ω_{CBOD}	m/d	0.01
α_{PC}	gP/gC	0.022	θ_{RE}	–	1.0241
f_{NH3}	–	0.50	θ	–	1.047
			θ_{SOD}	–	1.065

Table 3.4 Summary of model parameters for phytoplankton and zooplankton dynamics

Symbol	Unit	Value	Symbol	Unit	Value
p_{dz}	–	0.15	$K_{zm,max}$	1/d	0.005
p_{az}	–	0.85	h_L	W/m^2	177
$K_{ag,max}$	1/d	2.0	h_N	mg/L	0.01
$K_{zg,max}$	1/d	0.6–1.2	h_P	mg/L	0.005
$K_{ar,max}$	1/d	0.35	h_{gz}	mg/L	0.08
$K_{ae,max}$	1/d	0.0025	γ_0	m^{-1}	1.002
$K_{am,max}$	1/d	0.20	r_{CChla}	gC/gChl a	25.0
$K_{zr,max}$	1/d	0.005	θ	–	1.072
$K_{ze,max}$	1/d	0.0002	ω_a	m/d	0.05

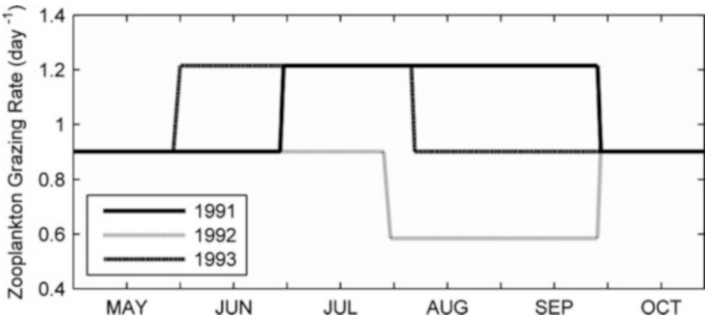

Fig. 3.6 Zooplankton grazing rates in the downstream reaches of the Tualatin River

10.1.3 Simulation Results

Figure 3.7 compares the measured and calculated water temperatures at Station RM16.2. Due to the use of 1-D heat transport equation, the simulated water temperature is cross-sectionally averaged. The field data obtained from [41] was collected at depths of 3, 6, 9, 12, 15, and 18 ft (1 ft = 0.3048 m) below the water surface. The cross-sectionally averaged water temperature is comparable to the measured water temperatures averaged over the depths, with 0.952 for R^2.

The depth-averaged reaeration rate K_{RE} and the sediment oxygen demand (SOD) are two key factors affecting DO concentration. The SOD in the main stem and several tributaries of the Tualatin River was measured in 1992–1994 during the summer period from May through October each year [44]. The temporally and spatially varied measurement SOD rates are used in the present simulation in 1992–1994, whereas the SOD rates in 1991 are unavailable and are approximated using the 1992 data. Because no measurement data for the reaeration rate, we tested the reaeration rate formulas of O'Connor and Dobbins (1958), Churchill et al. (1962), and Cadwallader and McDonnell (1969) by matching the simulated DO results with the measurement data. The simulated flow depths of the study reach in 1991–1993 range between 1.6 and 3.1 m and the flow velocities are approximately 0.02–1.2 m/s. According to the hydrodynamic properties of the river, the Churchill formula, $K_{RE} = 5.02Uh^{-1.67}$ (1/d), is suitable in this river reach and thus provides the simulated DO concentrations most comparable to the measurements. Here, U is the flow velocity in m/s and h is the water depth in m. The general trend of DO seasonal variation is reproduced by the model, as shown in Fig. 3.7, with R^2 of 0.606 when comparing the simulated and measured DO concentrations.

Figure 3.8 shows the temporal variations of simulated and measured ammonia and nitrate concentrations at RM5.5, and Fig. 3.9 presents the longitudinal profiles of mean concentrations of ammonia and nitrate averaged during the summer months May–October. The simulated and measured nitrogen concentrations agree well, with R^2 of 0.890 and 0.792 for ammonia and nitrate respectively. Measurement and simulation show low concentrations of ammonia in the upper reach from the upstream end to RM11.6. The ammonia and nitrate concentrations increase significantly at RM38.1 and RM9.3 due to the lateral discharges from the Rock

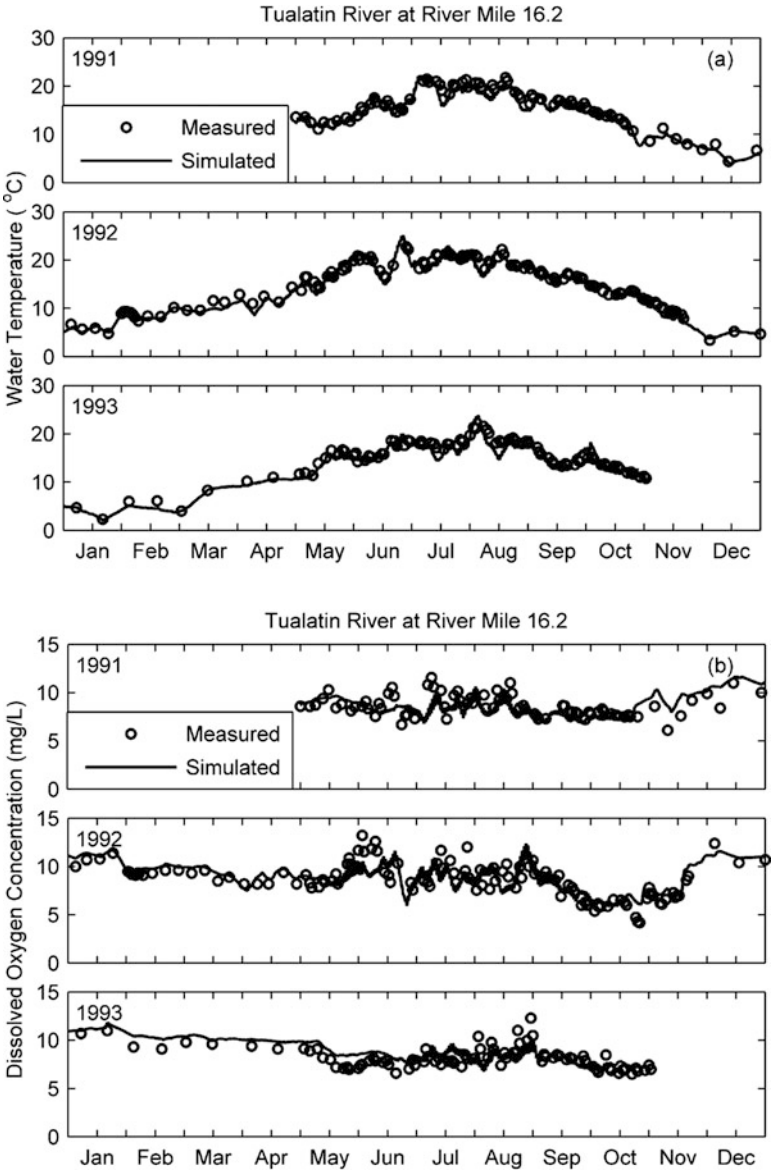

Fig. 3.7 Simulated vs. measured water temperature (**a**) and DO (**b**) concentrations at RM16.2 of the Tualatin River (measurements from Doyle and Caldwell [41])

Creek and Durham WWTPs. The figures show that the model can predict the variations of instream concentrations due to lateral inputs.

Figure 3.10 compares the simulated and measured temporal variations of phosphate concentrations at RM26.9 and longitudinal profiles of phosphate

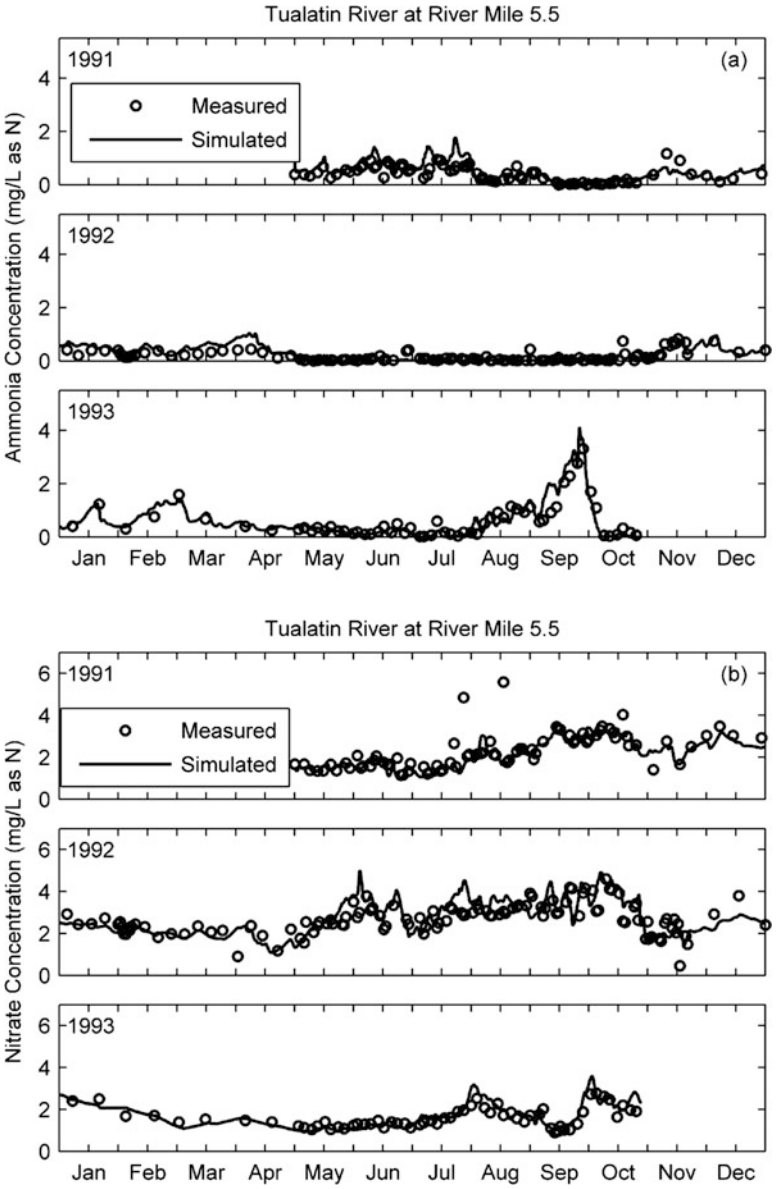

Fig. 3.8 Simulated vs. measured ammonia (**a**) and nitrate (**b**) concentrations at RM5.5

concentrations averaged over the summer months. The overall trend of simulated phosphate concentrations is comparable to the measurements, with R^2 of 0.922. In particular, reduction in the seasonally averaged concentration of phosphorus due to operation of the WWTPs at peak phosphorus-removal efficiency in 1992 [24] is presented in both measurement and simulation.

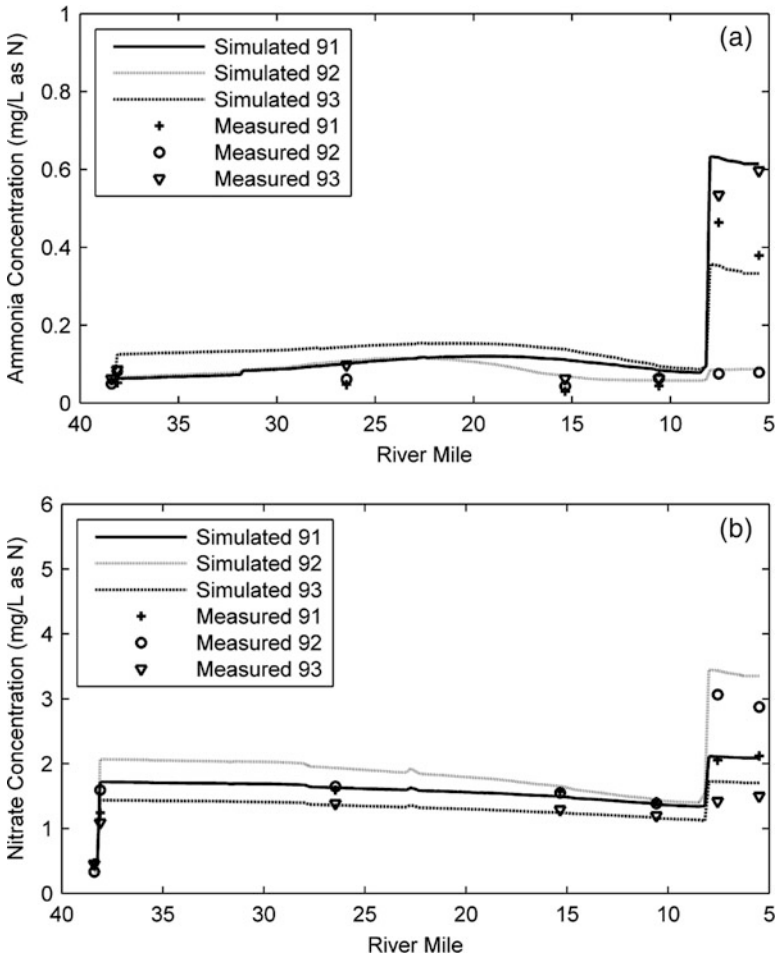

Fig. 3.9 Measured vs. simulated mean ammonia (**a**) and nitrate (**b**) concentrations during May–October

Figure 3.11 presents the comparison of the simulated and measured phytoplankton concentrations at RM5.5 and longitudinal profiles of phytoplankton biomasses averaged during the summer months. The simulation results and the field data are in a good agreement in the upstream locations. However, the simulated biomass in 1992 is much lower than the measurement in the downstream reaches. This may be due to the phytoplankton growth is limited by low concentration of phosphorus during this period. In addition, one can see that the model can predict the daily fluctuations due to the daily growth cycle.

The comparisons of measured and simulated zooplankton biomass at RM5.5 and other sections are presented in Fig. 3.12. The measured zooplankton concentrations have strong seasonal and interannual variability [35], especially at downstream

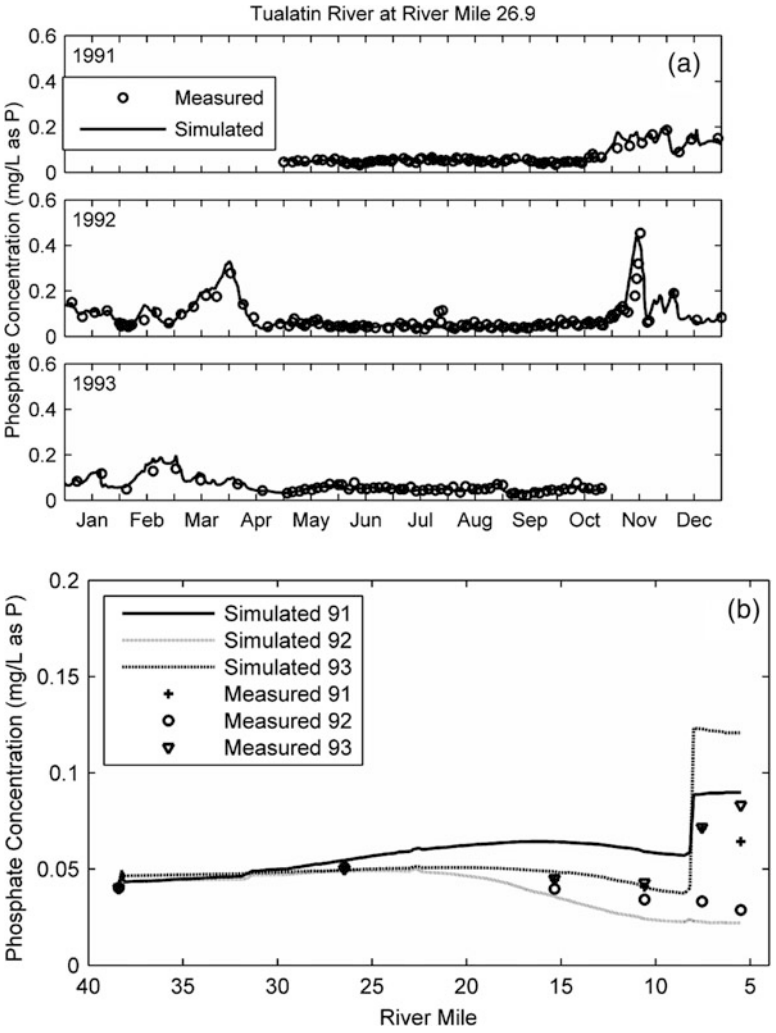

Fig. 3.10 Simulated vs. measured phosphate concentrations: (**a**) temporal variations at RM26.9 and (**b**) longitudinal profiles of mean values during May–October

locations. Using these calibrated grazing rates shown in Fig. 3.5, the model can reasonably reproduce the temporally and spatially varying zooplankton biomass, although the biomass peak at the RM5.5 during 1991 could not be observed. The calculated and measured zooplankton concentrations agree generally well, with $R^2 = 0.747$.

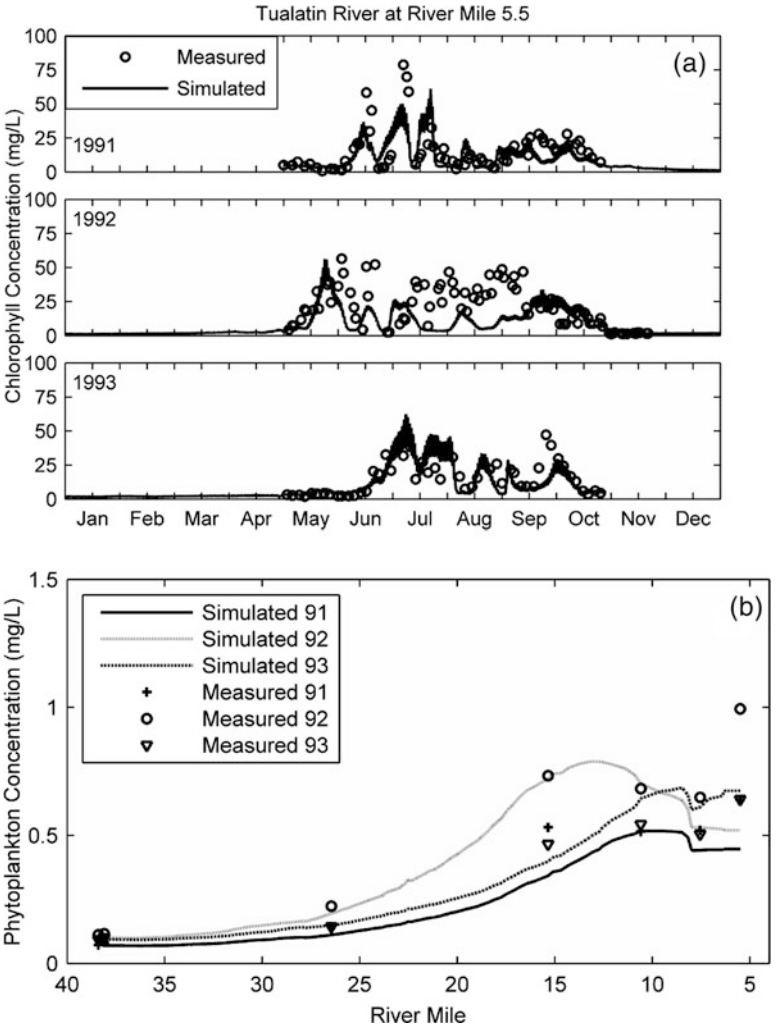

Fig. 3.11 Simulated vs. measured phytoplankton concentrations: (**a**) temporal variations at RM5.5 and (**b**) longitudinal profiles of mean values during May–October

10.2 Model Test in the Upper Hudson River, New York

10.2.1 Study Area

The Hudson River watershed encompasses 13,400 square miles in New York, Massachusetts, and Vermont, USA. The primary health risk of the river is the accumulation of PCBs discharged from plants of the General Electric Company that were located at Hudson Falls and Fort Edward. The reach is divided into the Upper and Lower Hudson River (UHR, LHR) by the Federal Dam at Troy. The UHR is a

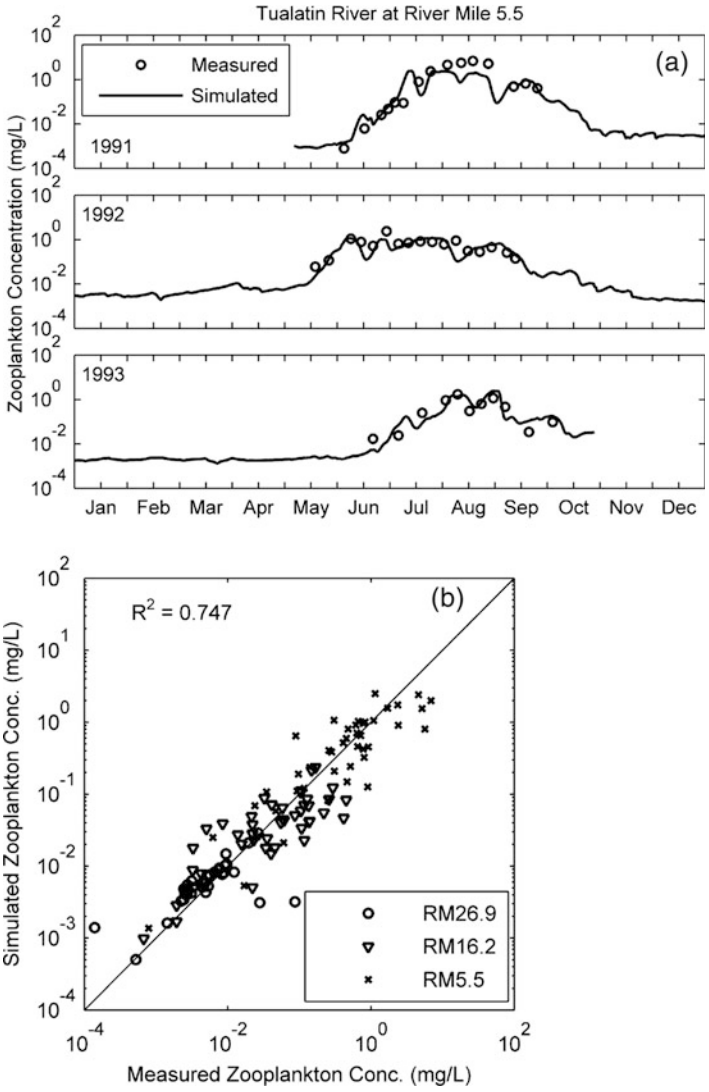

Fig. 3.12 Measured vs. simulated zooplankton concentrations: (**a**) temporal variations at RM5.5 and (**b**) comparison at three cross-sections

river-reservoir system comprised of a series of eight dams and associated backwater that extends from Fort Edward to Troy [45]. Due to the discontinuity along the river, each of the river reaches between the dams can be studied separately. The model developed in this study is applied to simulate the fate and transport of PCBs in a 13.3-mile reach of the UHR extending from Schuylerville (RM181.3) to Stillwater Dam (RM168.0), as shown in Fig. 3.13. The simulation domain is divided into 163 cross-sections. Each section is divided into 25 vertical panels.

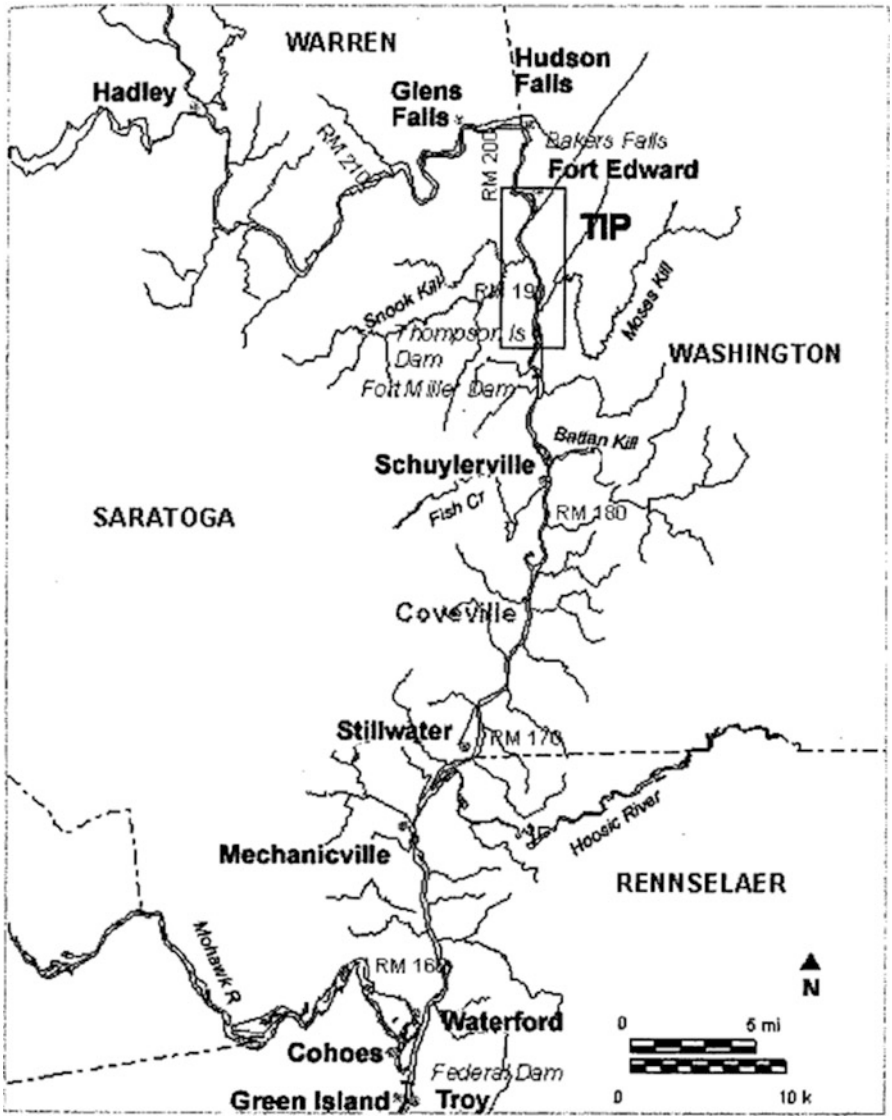

Fig. 3.13 Upper Hudson River (http://www.epa.gov/hudson/slide6.gif)

The simulation period is from March 1977 to December 1986. The time step is 15 min. The water velocities along the simulation domain range between 0.003 and 1.4 m/s with the average velocity of 0.37 m/s over the simulation period. The travel time is approximately 16 h. The study reach perhaps is too short to demonstrate the capability of modeling transport of water quality constituents, but it is a good case to test the model components of aquatic ecosystem and chemical bioaccumulation because of the controlled boundary conditions and abundant measurement data.

10.2.2 Model Inputs and Parameters

Discharge hydrograph from the USGS gauging station at Schuylerville and the staff gauge readings from the New York State Department of Transportation (NYSDOT) at the downstream location are used as boundary conditions for the hydrodynamic simulation. The upstream inflow is the main source for the flow discharge in the study reach. Small tributaries between Schuylerville and Stillwater are not considered in this study. Water quality of the UHR at Schuylerville and Stillwater were surveyed by New York State Department of Environmental Conservation (NYSDEC), and the data was reposited in STORET (STOrage and RETrieval) which is accessible through http://www.epa.gov/storet/. The times series of water quality constituents except phytoplankton measured at Schuylerville are used as the upstream inputs for water quality simulation. Because phytoplankton data is not available at Schuylerville, the phytoplankton biomass of the UHR at Waterford, which is located downstream of Stillwater, is used as the upstream phytoplankton loading. This substitution may contribute to errors in the model results.

The food web structure in the study reach can be divided to four trophic levels: phytoplankton, zooplankton, forage fish, and predatory fish. From 1976 to 1985, the New York State Department of Health (NYSDOH) conducted long-term biomonitoring studies using caddisfly and chironomid larvae as part of the Hudson River PCB Reclamation Demonstration Project [46]. The samplings were made in June through September of each year. The study showed that the most abundant taxa were chironomids and oligochaetes [45], which are used as the second trophic level representative in this study. Fish data were surveyed and collected using electrofishing by NYSDEC between 1970 and 1993, and weight, length, and the number of radius of annual growth rings on scales were measured. The number of fish caught in the Stillwater pool and the general detail of fish characteristics and behavior are published in [45]. Fish community of the UHR is composed of more than 30 species, which are classified into two groups: forage and predatory fish according to diet nature. The most common forage fish species are yellow perch, pumpkinseed fish, white sucker, golden fish, and brown bullhead. Large number of pumpkinseed fish is annually found in the study site starting from 1980, so that it is used as a representative for the forage fish in the model. The predatory fish species include largemouth bass and American eel. Largemouth bass is used to represent the predatory fish due to its general abundance.

The pathways of PCBs in aquatic organisms are the direct uptake from the water column and the transfer through food web via predation. A challenge to developing a modeling framework for PCB bioaccumulation is that PCBs consists of 209 individual congeners, which exhibit varying degrees of bioaccumulation potential [46]. The total PCB concentrations in fish were collected as part of NYSDEC monitoring program, and measured in fish on an Aroclor basis [45]. Therefore, the total PCBs is considered in the present model for simplicity.

The water quality model parameters in the UHR case are similar to those in the Tualatin River case shown in Tables 3.3 and 3.4 [42]. The feeding preference of the

Table 3.5 Preference consumption of the UHR food web model

Species	Detritus	Phytoplankton	Zooplankton	Forage fish	Predatory fish
Zooplankton	0.15	0.85	–	–	–
Forage fish	0.15	0.25	0.5	0.1	–
Predatory fish	0.025	0.175	0.25	0.85	0.15

Table 3.6 Summary of some model parameters used for the UHR ecological model

Symbol	Unit	Value	Symbol	Unit	Value
$K_{ag,max}$	1/d	1.0	e_{fg}	–	0.75
$K_{ar,max}$	1/d	0.25	a_f	–	0.45
$K_{am,max}$	1/d	0.35	b_f	–	−0.36
ω_a	m/d	0.25	W_p	g	525
$K_{zg,max}$	1/d	0.75	$K_{pb,max}$	1/d	0.99
$K_{zr,max}$	1/d	0.015	$K_{pm,max}$	1/d	0.002
$K_{zm,max}$	1/d	0.035	e_{pg}	–	0.70
e_{zg}	–	0.7	a_p	–	0.33
W_f	g	380	b_p	–	−0.325
$K_{fb,max}$	1/d	0.9	T_{opt}	°C	22.5
$K_{fm,max}$	1/d	0.0015	θ	–	1.072

Table 3.7 Summary of some model parameters used for the UHR ecotoxicological model

Species	K_1 (1/d)	K_2 (1/d)	LC50 (μg/L)	t_1 (h)
Phytoplankton	1.0E-7	5.0E-4	1E-8	24
Zooplankton	1.0E-7	5.0E-5	31	96
Forage fish	5.0E-4	2.5E-3	2740	96
Predatory fish	7.5E-5	5.0E-3	236.4	96

UHR food web model is presented in Table 3.5. The selected model parameters used in ecological and ecotoxicological models are shown in Tables 3.6 and 3.7. These model parameters obtained from several literature sources, such as [2, 10, 34, 35].

10.2.3 Simulation Results

The comparisons of simulated results and field data of ammonia, nitrate, phosphate, DO and CBOD at Stillwater are shown in Figs. 3.14 and 3.15. Because lateral inflows from tributaries and fields are not taken into account in this study, the simulation results largely depend on the nutrient concentrations of the upstream input. From Schuylerville to Stillwater, the river flows mostly through suburban and agricultural areas, and the usage of fertilizer might contribute to the measured instream nutrient of the river. Nevertheless, the simulation results and field data of water quality are in generally good agreement, with R^2 of 0.856, 0.665, 0.495, 0.865 and 0.514 for ammonia, nitrate, phosphate, DO and CBOD, respectively.

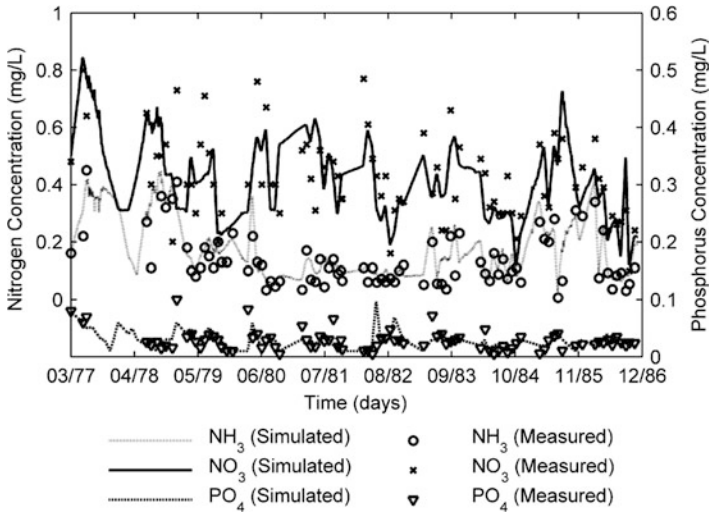

Fig. 3.14 Simulated and measured ammonia, nitrate, and phosphate concentrations at Stillwater (measurements from NYSDEC)

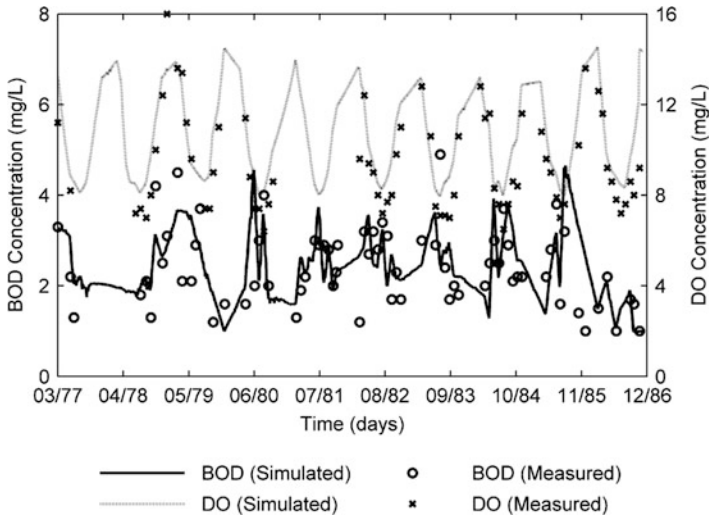

Fig. 3.15 Simulated and measured DO and BOD concentrations at Stillwater (measurements from NYSDEC)

The simulated and measured biomass concentrations of zooplankton, forage fish and predatory fish at Stillwater are shown in Fig. 3.16. The simulation shows annual zooplankton biomass peaks, which may be caused by the seasonal growth of phytoplankton. Although zooplankton in August 1983 is under-estimated, its biomass concentrations estimated over 11-year simulation period are consistent with

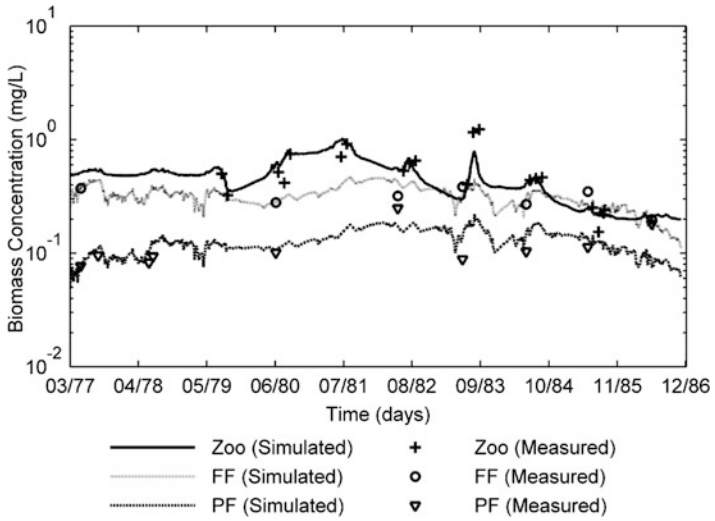

Fig. 3.16 Simulated and measured zooplankton (Zoo), forage fish (FF), and predatory fish (PF) biomass concentrations at Stillwater (measurements from NYSDEC)

the field measurements. The simulated biomasses of forage fish are comparable to the survey data. The numerical results of the predatory fish in 1982 and 1986 are lower than the measurements. One of the reasons is that from the field record, American eel was caught only in 1982 and 1986, and there is no evidence to show the cause of its nonexistence for other years. Therefore, the measured total biomass of the top predators including largemouth bass and American eel suddenly increases in 1982 and 1986. In addition, the initial fish biomass in 1977, which is used for modeling setup, is only the biomass of largemouth bass. It means that there is no American eel at the beginning of the simulation, and the model basically simulates the biomass of largemouth bass for the entire simulation period. Without considering American eel, the simulated results are more comparable to the measurement data. Moreover, the model assumes that fish did not leave the system because the downstream end of the study reach is the Stillwater Dam. Since the predatory fish is considered as the top trophic level, the biomass loss depends solely on non-predatory and gamete mortalities as well as defecation of unassimilated food. In reality, they can be consumed by other animals, caught by humans, or leave the system domain. These unconsidered factors may contribute to the difference between the simulation results and measurements. Other factors include the lack of data and uncertainties in the real nature.

Figure 3.17 compares the simulated and measured total PCB concentrations in the water column at Stillwater, and the general trend is reproduced well by the model. Figure 3.18 compares the simulated and measured PCB concentrations in pumpkinseed and largemouth bass, which are used as representatives for forage and predatory fish, respectively. The adult largemouth bass samples were collected in Spring, while small pumpkinseed were collected in late Summer or early Fall. The

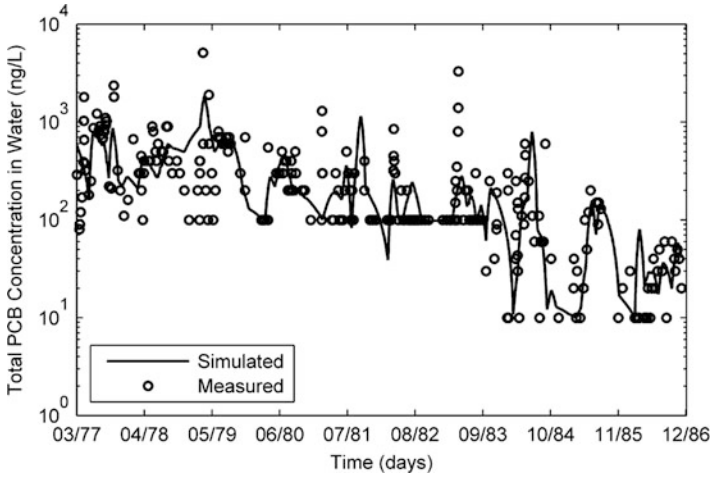

Fig. 3.17 Simulated and measured the total PCB concentrations in water column at Stillwater (measurements from USGS)

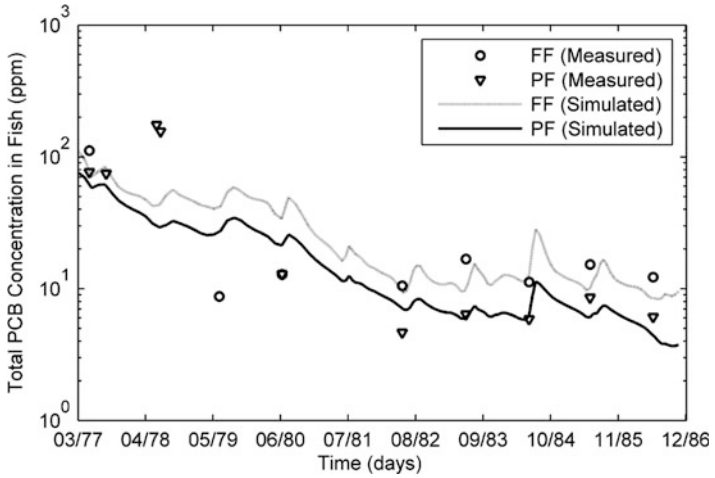

Fig. 3.18 Simulated and measured total PCB concentrations in fish at Stillwater (measurements from NYSDEC)

PCB levels in pumpkinseed slowly decline from the late 1970s to 1982. Slight fluctuation of PCB is observed after 1982. Similar to pumpkinseed, the PCB concentrations in largemouth bass gradually decrease until 1982 and are subsequently steady. The results show that the model is able to predict reasonably well the bioaccumulation of PCB in both fish species, with R^2 of 0.425 and 0.373.

11 Conclusions

An integrated one-dimensional modeling package has been developed to simulate hydrodynamic, sediment transport, water quality, aquatic ecosystem and ecotoxicology in river systems. The model simulates the temporal and spatial variations of the concentrations of water quality constituents and biotic organisms. The simulated water quality constituents include water temperature, DO, CBOD, nitrogen, phosphorus, and conservative chemical such as chloride. The used food web consists of four trophic levels: phytoplankton, zooplankton, forage fish, and predatory fish, which undergo the biological processes of photosynthesis, grazing, respiration, excretion, defecation, mortality, gamete, and reproduction. The model simulates the bioaccumulation of toxic chemicals in aquatic organisms through direct uptake from water, depuration and dietary, and takes into account the toxicity effects through modification factors for the growth, grazing, and gamete mortality of the organisms.

The developed model is applied to simulate water quality in the Tualatin River, Oregon, which has high influences of lateral inputs from wastewater treatment plants and tributary discharges. The model reproduces well the time-series concentrations of water quality constituents and biomass of phytoplankton and zooplankton in the Tualatin River. The model is also applied to simulate the water quality, aquatic ecosystems, as well as fate and transport of the total PCB concentrations in the water column and aquatic organisms in the Upper Hudson River (UHR), New York. The simulated water quality parameters, zooplankton biomass, fish populations, and total PCBs concentrations in both forage and predatory fish are in generally good agreement with the measurement data.

The developed model is comparable to the WASP model in terms of water quality modeling, and has the basic features but is much simpler than the AQUATOX model in terms of aquatic ecology and ecotoxicology modeling. It is integrated with a well-developed model of flow and sediment transport in channel networks. It is relatively more convenient to use in assessment of the impacts of flood, river restoration, dam construction, morphological change, chemical spill and etc. on river ecosystems.

References

1. Jørgensen, S. E. (1980). *Lake management*. New York: Pergamon Press.
2. Di Toro, D. M., Fitzpatrick, J. J., & Thomann, R. V. (1981). *Water Quality Analysis Simulation Program (WASP) and Model Verification Program (MVP) Documentation* (EPA/600/3-81/044). Washington, DC: U.S. Environmental Protection Agency.
3. Wool, T. A., Ambrose, R. B., Martin, J. L., & Comer, E. A. (2001). *The Water Quality Analysis Simulation Program, WASP6. Part A: Model documentation*. Athens, GA: U.S. Environmental Protection Agency, Center for Exposure Assessment Modeling.

4. Chapra, S. C., Pelletier, G. J., & Tao, H. (2008). *QUAL2K: A modeling framework for simulating river and stream water quality, version 2.11: Documentation and users manual*. Medford, MA: Civil and Environmental Engineering Department, Tufts University.
5. Cerco, C., & Cole, T. (1994). *Three-dimensional eutrophication model of Chesapeake Bay* (Technical Report EL-94-4). Vicksburg, MS: U.S. Army Engineer Waterways Experiment Station.
6. Chao, X., Jia, Y., & Zhu, T. T. (2006). *CCHE_WQ water quality module* (Technical Report No. NCCHE-TR-2006-01). Oxford, MS.
7. Christensen, V., & Walters, C. J. (2004). Ecopath with ecosim: Methods, capabilities, and limitations. *Ecological Modelling, 172*, 109–139.
8. Hipsey, M. R., Romero, J. R., Antenucci, J. P., & Hamilton, D. (2006). *Computational aquatic ecosystem dynamics model: CAEDYM v2* (WP 1387.1 MH). Australia.
9. Ulanowicz, R. E. (2006). *EcoNetwrk – A user's guide*. http://www.glerl.noaa.gov/EcoNetwrk (accessed in 2009).
10. Park, R. A., & Clough, J. S. (2004). *AQUATOX (release 2) modeling environmental fate and ecological effects in aquatic ecosystems. Volume 2: Technical documentation* (EPA-823-R-04-002). Washington, DC: Office of Water, U.S. Environmental Protection Agency.
11. Park, R. A., & Clough, J. S. (2009). *AQUATOX (release 3) modeling environmental fate and ecological effects in aquatic ecosystems. Volume 2: Technical documentation* (EPA-823-R-09-004). Washington, DC: Office of Water, U.S. Environmental Protection Agency.
12. Bahadur, R., Amstutz, D. E., & Samuels, W. B. (2013). Water contamination modeling – A review of the state of the science. *Journal of Water Resource and Protection, 5*, 142–155.
13. Sharma, D., & Kansal, A. (2013). Assessment of river quality models: A review. *Reviews in Environmental Science and Bio/Technology, 12*(3), 285–311.
14. Zhang, W., & Rao, Y. R. (2012). Application of a eutrophication model for assessing water quality in Lake Winnipeg. *Journal of Great Lakes Research, 38*(3), 158–173.
15. Zhang, L., Liu, J., Li, Y., & Zhao, Y. (2013). Applying AQUATOX in determining the ecological risk assessment of polychlorinated biphenyl contamination in Baiyangdian Lake, North China. *Ecological Modelling, 265*, 239–249.
16. Scholz-Starke, B., Ottermanns, R., Rings, U., Floehr, T., Hollert, H., Hou, J., et al. (2013). An integrated approach to model the biomagnification of organic pollutants in aquatic food webs of the Yangtze Three Gorges Reservoir ecosystem using adapted pollution scenarios. *Environmental Science and Pollution Research, 20*(10), 7009–7026.
17. Joyner, T. A., & Rohli, R. V. (2013). Atmospheric influences on water quality: A simulation of nutrient loading for the Pearl River Basin, USA. *Environmental Monitoring and Assessment, 185*(4), 3467–3476.
18. Karaaslan, Y., Akkoyunlu, A., Erturk, F., & Citil, E. (2013). The effect of toxic organic chemicals on Mogan lake. *International Journal of Environmental Research, 7*(3), 595–604.
19. Chen, Y., Niu, Z., & Zhang, H. (2013). Eutrophication assessment and management methodology of multiple pollution sources of a landscape lake in North China. *Environmental Science and Pollution Research, 20*(6), 3877–3889.
20. Ambrose, R. B., & Wool, T. A. (2009). *WASP7 stream transport – Model theory and user's guide, Supplement to Water Quality Analysis Simulation Program (WASP), user documentation* (EPA/600/R-09/100). Washington, DC: U.S. Environmental Protection Agency.
21. Tsegaye, T., & Wagaw, M. (2007). *Stream water quality modeling using AQUATOX*. National Water Quality Meeting, Savannah, GA.
22. Wu, W., & Vieira, D. A. (2002). *One-dimensional channel network model CCHE1D version 3.0 – Technical manual* (Technical Report No. NCCHE-TR-2002-1). Oxford, MS.
23. Vieira, D. (2004). *Integrated modeling of watershed and channel processes*. Oxford, MS: National Center for Computational Hydroscience and Engineering, The University of Mississippi.
24. Wu, W. (2007). *Computational river dynamics*. New York: Taylor & Francis.
25. Tennessee Valley Authority. (1972). *Heat and mass transfer between a water surface and the atmosphere*. Division of Water Control Planning.

26. Deas, M. L., & Lowney, C. L. (2000). *Water temperature modeling review*. Central Valley, CA.
27. Genetti, A. J. J. (1998). *Engineering and design – Runoff from Snowmelt*. Washington, DC: U.S. Army Corps of Engineers.
28. Kaushik, C. P., Bhavikatti, S. S., & Kaushik, A. (2010). *Basic civil and environmental engineering*. New Delhi, India: New Age International.
29. Chapra, S. (1997). *Surface water-quality modeling*. New York: McGraw-Hill.
30. Haider, H., Ali, W., & Haydar, S. (2012). Evaluation of various relationships of reaeration rate coefficient for modeling dissolved oxygen in a river with extreme flow variations in Pakistan. *Hydrological Processes*. doi:10.1002/hyp.9528.
31. Liu, W.-C., & Chen, W.-B. (2012). Monitoring sediment oxygen demand for assessment of dissolved oxygen distribution in river. *Environmental Monitoring and Assessment, 184*(9), 5589–5599.
32. Brown, L. C., & Barnwell, T. O. (1987). *The enhanced stream water quality model QUAL2E and QUAL2E-UNCAS: Documentation and user manual*. Athens, GA.
33. Xu, K., Jiang, H., Juneau, P., & Qiu, B. (2012). Comparative studies on the photosynthetic responses of three freshwater phytoplankton species to temperature and light regimes. *Journal of Applied Phycology, 24*(5), 1113–1122.
34. Bowie, G. L., Mills, W. B., Porcella, D. B., Campbell, C. L., Pagenkopf, J. R., Rupp, G. L., et al. (1985). *Rates, constants, and kinetics formulations in surface water quality modeling* (EPA/600/3-85/040). Athens, GA: U.S. Environmental Protection Agency.
35. Rounds, S. A., Wood, T. M., & Lynch, D. D. (1999). *Modeling discharge, temperature, and water quality in the Tualatin River, Oregon*. USGS Water Supply Paper; 2465-B, U.S. Geological Survey, Oregon.
36. Kitchell, J. F., Koonce, J. F., O'Neill, R. V., Shugart, H. H., Jr., Magnuson, J. J., & Booth, R. S. (1974). Model of fish biomass dynamics. *Transactions of the American Fisheries Society, 103*, 786–798.
37. Leidy, G. R., & Robert, M. J. (1977). *The development of fishery compartments and population rate coefficients for use in reservoir ecosystem modeling* (Contract Rept. CR-Y-77-1, 134 pp.). Vicksburg, MS: U.S. Army Engineer Waterways Experiment Station.
38. Di Toro, D. M. (2001). *Sediment flux modeling*. New York: Wiley.
39. Thomann, R. V., & Connolly, J. P. (1984). *An age dependent model of PCB in a Lake Michigan food chain*. New York: Manhattan College.
40. Connolly, J. P., Zahakos, H. A., Benaman, J., Ziegler, K. C., Rhea, J. R., & Russell, K. (2000). A model of PCB fate in the Upper Hudson River. *Environmental Science & Technology, 34*, 4076–4087.
41. Doyle, M. C., & Caldwell, J. M. (1996). *Water-quality, streamflow, and meteorological data for the Tualatin River Basin, Oregon, 1991–1993* (Open-File Report 96-173). Portland, OR: U.S. Geological Survey.
42. Inthasaro, P. (2010). *A one-dimensional aquatic ecology and ecotoxicology model in river systems*. PhD dissertation, National Center for Computational Hydroscience and Engineering, The University of Mississippi, Mississippi.
43. Thomann, R. V., & Mueller, J. A. (1988). *Principles of surface water quality modeling and control*. New York: Harper & Row.
44. Rounds, S. A., & Doyle, M. C. (1997). *Sediment oxygen demand in the Tualatin River basin, Oregon, 1992–96* (Water-Resources Investigations Report 97-4103). Portland, OR: U.S. Geological Survey.
45. QEA. (1999). *PCBs in the Upper Hudson River Volume 2: A model of PCB fate, transport, and bioaccumulation*.
46. TAMS Consultant, Limno-Tech, Menzie-Cura & Associates, & Tetra Tech. (2000). *Volume 2D – Revised baseline modeling report: Hudson River PCBs reassessment RI/FS*, Book 3 of 4 – Bioaccumulation models. New York.